Front. Phys. China, 2008, 3(2): 126–152
DOI 10.1007/s11467-008-0018-y

REVIEW ARTICLE

Yun ZHANG

Generation of non-classical states from an optical parametric oscillator/amplifier and their applications

Abstract Quantum information and quantum optics are rapidly advancing areas of modern physics. As an important device in quantum optics and quantum information, the optical parametric amplifier/oscillator (OPA/O) has been extensively studied and applied to the generation of non-classical state since the 1980s. This article reviews the progress in the generation of non-classical state from an OPO/A and application of twin beams in quantum optics and quantum information.

Keywords entanglement, optical parametric oscillator, squeezed state, twin beams

PACS numbers 42.50.Dv, 42.25.-p, 03.67.Dd

1 Introduction

Non-classical states or quantum states are arguably the important resource in the field of quantum information [1, 2] and quantum optics. The most well-known non-classical state of light is the so-called squeezed state. It is special since its optical noise is redistributed such that its noise is less than the standard quantum noise limit in one quadrature while the fluctuations are larger in the correspondingly orthogonal quadrature. Another non-classical state is the twin beams state, in which intensity difference fluctuations between them is less than that between two coherent beams. In addition, entanglement, i.e., nonlocal quantum correlation between two or more quantum mechanical objects, is the essential resource in present quantum information and communications technology. Furthermore, it has also been used to verify the foundations of the quantum theory. Thus, the development of techniques to generate these quantum states is of great importance in this field. Lots of efficient methods have been proposed to generate the non-classical state. Among them, two of the most successful systems for squeezed state generation have been the optical parametric oscillator (OPO) and optical parametric amplifier (OPA), both of which have the same underlying the second-order ($\chi^{(2)}$) nonlinearity. With the $\chi^{(2)}$ nonlinearity, the two-photon state from spontaneous parametric down-conversion (SPDC) has served as a test bed for verifying the foundations of the quantum theory, such as the Einstein, Podolsky and Rosen (EPR) paradox [3], and has been exploited as a powerful source for demonstrating quantum information experiments with discrete variable [4]. On the other hand, OPA/O has also developed into one of the most efficient tools to produce entangled states and squeezed state of light for quantum information systems with continuous variable (CV) from the first realization of squeezed state from an OPO at a couple of decades ago.

The operation regime for the above device is one in which the OPO is pumped by a harmonic wave (frequency $2\,\omega$), whose power is close to the threshold power for the onset of parametric oscillation. The input subharmonic waves are usually either vacuum modes or very weak, so that in the amplification process no or very little power is transferred to them from the pump wave (no pump deletion). Basic optical processes of OPO involving the $\chi^{(2)}$ nonlinearity are illustrated in Fig. 1. We

Yun ZHANG[1,2] (✉)

[1] Department of Physics, Gakushuin University, 1-5-1 Mejiro, Toshima-ku, Tokyo, 171-8588, Japan
[2] CREST, Japan Science and Technology Agency, 1-9-9 Yaesu, Chuo-ku, Tokyo, 103-0028, Japan
E-mail: zhangyun@qo.phys.gakushuin.ac.jp

Received February 14, 2008; accepted March 1, 2008

note that a common feature of these processes is that it involves the interaction of three waves, $\chi^{(2)}$ processes are therefore also known as three-wave mixing processes. The processes can be divided into two categories according to the features of two sub-harmonic outputs: The degenerate processes, where all the features of two sub-harmonic photons are identical and non-degenerate processes where at least one feature of two sub-harmonic photons (such as frequency in Fig. 1) is different from each other. Unlike another $\chi^{(2)}$ process, which is called second harmonic process (SHG), these processes have associated threshold powers above which the dissociation of a 2ω photon into the sub-harmonic photons with frequency of ω occurs. These processes are called degenerate and non-degenerate optical parametric oscillator (DOPO and NDOPO). Below the threshold, the dissociation of a 2ω does not occur; however, we can trigger the dissociation of the 2ω photons by injecting a seeder. These processes are called optical parametric amplification. We can also think of the below threshold DOPO and NDOPO as being vacuum seed, that is to say it is the fluctuations of the vacuum field which trigger the dissociation of the 2ω photons.

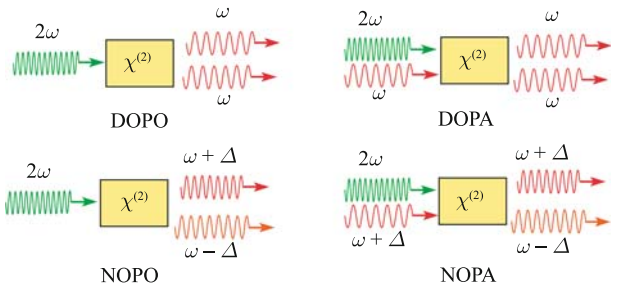

Fig. 1 Overview of the down conversion processes. Degenerate and non-degenerate optical parametric oscillations are shown. By introduction of a seed field, it shows the process of degenerate and non-degenerate optical parametric amplifications.

In a degenerate mode, the above device has proved to be the most efficient source of single-mode quadrature squeezed light. Efficient generation of vacuum squeezing, low power amplitude squeezing, high power (bright) amplitude squeezing or phase squeezing has been obtained by the DOPO without injected sub-harmonic signal or the DOPA with injected sub-harmonics signal. In a non-degenerate mode, the NDOPO can generate two separable quantum correlated fields which can be used to create two-mode vacuum squeezing and strong EPR entanglement or quantum correlated twin beams when it is operating below or above its threshold, respectively. Similarly to DOPA, the bright two-mode squeezing was also generated from a NDOPA with injected sub-harmonic signal operating below its threshold. Recently, the implementation of NDOPO is focused on the realization of EPR paradox when it is operating above threshold. Although the initial proposal has been proposed about twenty years ago by Reid and Drummond [5, 6], the particular implementation has been carried out only recently [7−9].

To operate OPO/OPA, both the continuous wave (cw) and pulsed laser can be utilized as the light source. When a cw laser is used, a cavity is usually employed to enhance the nonlinear interaction. Also, the bandwidth of the generated non-classical state is limited by the linewidth of resonant cavity. On the other hand, the fundamental advantage of pulsed experiments is that it enables to generate a broad bandwidth squeezed state. The high intensity during a pulse and consequently the very large nonlinear effects that can occur, makes the build-up cavities, which are necessary in cw experiments, obsolete. However, the high intensities of pulsed operation can introduce at the same time other nonlinear processes, such as self focusing, gain induced diffraction, which produces distortions of the wave fronts of the amplified signals, and make the detection of squeezed light very difficult.

In this review article, our objective is to review in detail the generation of all kinds of non-classical state from OPO/OPA, while providing an overview of related achievements that enable both a historical perspective and a future outlook. The organization of this paper is as follows: In Section 2, we first give a historical summary of generation of non-classical state from OPA/O. Since the first demonstration of the squeezed state in 1985, we have seen a steady improvement in the size and the reliability of the noise suppression. Some landmark achievement will be introduced in this section. Section 3 is devoted to some classical properties of OPO. To characterize the OPA/O, the initial properties of OPO are the classical properties. In this section, the threshold, relaxation oscillation and classical gain, which are related to the generation of non-classical state, are discussed in experiment. We present two experiments of the generation of squeezed state from OPA in Section 4. One experiment reports the generation of a 3.4 dB signal mode squeezed state with a single pass through OPA, in which a periodically poled lithium niobate waveguide is used as a nonlinear material and pulse laser was employed as light source; another experiment reports the generation of two-mode squeezed state from a NOPA with an enhanced cavity. The light source is an amplified and noise suppressed diode laser. The experiment of the generation of twin beams is discussed in Section 5. In Section 6, we turn to the detail of the generation of entanglement from OPA/O. We give an experiment on the generation

of entanglement by combing two squeezed vacua, and review the generation entanglement state from a below threshold NDOPA or above threshold NDOPO. Before the summary and outlook in Section 8, we present some of applications of twin beams in Section 7. A quantum communication channel experiment has been performed based on the measurement of photon-number difference.

2 Chronology of generation non-classical state from OPO

The starting point for a description of non-classical state originates with coherent states, theoretically proposed by Glauber [10]. In quantum optics, an optical field is quantized with annihilation and creation operator $\hat{a}$ and $\hat{a}^\dagger$, which are decomposed into two Hermitian operators $\hat{x}$ and $\hat{p}$ in the form of $\hat{a} = (\hat{x}+\mathrm{i}\hat{p})/2$ and $\hat{a}^\dagger = (\hat{x}-\mathrm{i}\hat{p})/2$. $\hat{x}$ and $\hat{p}$, the real and imaginary parts of the complex amplitude, give dimensionless amplitudes for the modes' two quadrature phases. They obey the communication relation of $[\hat{x},\hat{p}] = 2\mathrm{i}$ and correspond to the uncertainty principle of $\Delta^2 x\Delta^2 p \geqslant 1$, in which $\Delta^2 A$ is variance of observable $\hat{A}$ defined by $\Delta^2 A = \langle\hat{A}^2\rangle - \langle\hat{A}\rangle^2$. The relation with the equals sign defines a family of minimum-uncertainty states. The coherent state with $\Delta^2 x = \Delta^2 p = 1$ is a special case with equal variances in its two quadrature phases. In optics measurement, it was called shot noise limit (SNL) or quantum noise level (QNL). We can reduce variance in one quadrature at the expense of increasing variance in the other ($\Delta^2 x < 1 < \Delta^2 p$). Such states we shall call squeezed state. It may be generated by using OPO/OPA. In addition to the generation of squeezed state, the above-threshold NDOPO produces two identical beams, which is called signal and idler beams with annihilation operator $\hat{a}_s$ and $\hat{a}_i$, respectively. The intensity difference variance has a property of $\Delta^2(\hat{a}_s^\dagger\hat{a}_s - \hat{a}_i^\dagger\hat{a}_i) < \Delta^2(\hat{a}_1^\dagger\hat{a}_1 - \hat{a}_2^\dagger\hat{a}_2)$, where $\hat{a}_1$ and $\hat{a}_2$ are annihilation operators of two coherent states, respectively. This state is named twin beams [11]. Entanglement describes the quantum correlation between two or more objects. Sufficient criteria for the existence of bipartite quantum entanglement of continuous variable between modes A and B are proposed [12, 13]. One of the most convenient criteria for experimentalists is $\Delta^2(\hat{x}_A - \hat{x}_B) + \Delta^2(\hat{p}_A + \hat{p}_B) < 2$. Of course, the left-hand side of this equation is zero for the perfect EPR state. With this criterion, we can check the existence of entanglement between modes A and B in the state.

In 1985 a team from Bell Labs led by Slusher [14] found the first experimental evidence of squeezing by using a four-wave mixing process induced by the nonlinear susceptibility of a sodium atomic beam. The amount of squeezing of 25 % was modest. Soon after that, generation of squeezed state from a below threshold OPO was carried out and 63 % of squeezing was obtained [15, 16]. Due to the stability of the system and potential application to gravitational wave detection, the generation of squeezed state from OPO/OPA was extensively studied both in experiment and theory. Furthermore, applications of squeezed state, such as sub-shot-noise measurement, quantum non-demolition measurement and atomic spectroscopy, were rapidly developed. During the last few years, squeezed state is considered the most important resource for future quantum information technology with continuous variable.

All the applications of non-classical state rely on a stable, reliable, strong and flexible squeezing source. Triggered by those requirements, progress in the development of practical sources of squeezed light has been concentrated on technical issues, such as improving stability of the system and increasing the squeezing level. Up to now, lots of experiments are performed in different media and geometries, and some remarkable achievements are accomplished. The most remarkable achievement, we believe, is that the noise suppression of 3.8 dB in the sub-harmonic output wave was recorded continuously for more than four hours [17]. Later, both noise suppression and the stability was further improved up to 6.2 dB and 36 hours [18], respectively. In this system, a seed wave is resonantly injected for stabilizing the phase between the pump and seeder. Because of the semi-monolithic OPO cavity configuration and reliability of the electronic lock systems long-term stability of the device was achieved.

With the improvement of the amount of noise suppression, since the first experimental demonstration of squeezed light succeeded in 1985, dedicated research in the succeeding two decades could only elaborate typical factors of 3 dB to 6 dB. However, very recently, a great step forward was achieved at the University of Tokyo and quantum noise squeezing of 9 dB at 860 nm was observed by suppression of the phase fluctuation of LO and the reduction of the intracavity losses [19]. It was quickly beaten by a group led by Schnabel in Germany with a noise reduction of 10 dB by employing a monolithic OPO cavity, which has minimum intracavity losses [20]. To the twin beams, since the experiments involve only intensity measurements, and without local oscillator (LO), it seems a little easier. The noise reduction of 8.5 dB [21], which is a record that stood for a long time, was observed soon after the first twin beams experiment. It was beaten by the group at Shanxi University with a noise suppression of 9.2 dB [22] and finally improved

again to 9.5 dB by the group led by Fabre in 2005 [23].

In addition, the achievements on the generation of squeezed states in the audio signal band [24] and generation of squeezed states using frequency doubled laser diode as light source [25] were attractive achievements. The former provides an important step for the stable application of squeezed light in gravitational wave detectors; and the latter makes it easier to realize the tunable squeezed source and further compact the system.

Another landmark experiment was the test of EPR paradox with continuous variable. The first experiment to produce continuous variable broadband EPR correlations [26, 27] was performed by Ou *et al.* In their experiment, the EPR beams were generated using a subthreshold nondegenerate type II intracavity OPO in a manner proposed by Reid and Deummond [5]. Such a system consists, conceptually, of a type II nonlinear process in which pump photons at some frequency of Ω_p are converted to pairs of correlated signal and idler photons with degenerate frequency of $\Omega_s = \Omega_i = \Omega_p/2$ frequency and nondegenerate orthogonal polarization. In the experiment of Ou *et al.*, the nonlinear effect of nonlinear medium was enhanced by placing it inside resonant cavities for each of the pump, signal, and idler fields. The pump field at 540 nm was generated by an intracavity frequency doubled Nd:YAP laser, and the nonlinear medium was a type II non-critically phase matched KTP crystal. The signal and idler fields produced by the NDOPO, were analyzed in a pair of homodyne detectors. Strong correlations were observed between the output photocurrents both for joint amplitude quadrature measurement and phase quadrature measurement.

In Table 1 we present a history of generation of nonclassical state from OPO/OPA, an extension of a list given earlier in a paper by Anderson [28]. In the table we indicate the system that was used, the amount of squeezing, the wavelength of squeezed state and nonlinear crystal that was used. Some important experiments may be excluded, but it clearly brings out the development of the generation squeezed state from OPO/OPA over two decades.

From the table, we see that the magnitudes of the best squeezing results have been steadily increased. However, what is not reflected in the table is that the increase in the reported squeezing also comes with a corresponding increase in the stability of the generated squeezing: From the observation of a few milliseconds of fluctuations lower than SNL in many experiments where subquantum noise behavior of light was continuously and stably observed for many hours. Both of these trends were brought about by advances in the many requisite technologies for a squeezing experiment: The availability of ultra-stable pump lasers (e.g. non-planar ring oscillator Nd:YAG laser); The discovery of new nonlinear crystal materials (e.g. PPKTP) and innovations in crystal growing, polishing and coating techniques; The invention and refinement of new stable locking techniques for optical experiments. However, the most important ef-

Table 1 History of experimental generation of non-classical state from OPO/OPA.

Refs.	System	Squeezing/%	Wavelength/nm	Medium	Note
[15, 16]	Below-threshold OPO	63	1064	$LiNbO_3$	SMSS
[29]	Below-threshold OPO	37	1064	KTP	TMSS
[30]	Pulsed squeezing, OPO	13	1064	KTP	TMSS
[31]	Above-threshold OPO	30	1067,1048	KTP	TB
[32]	Above threshold OPO	54	1012,1120	$MgO:LiNbO_3$	TB
[33]	Incoherent pulse, OPO	17	1064	KTP	TMSS
[34]	Pulsed squeezing,OPO	22	1064	$Ba_2NaNb_5O_{15}$	SMSS
[35]	Pulsed twin beams	80	1064	KTP	TB
[36]	Josephson parametric amplifier	47	(19.16 GHz)		SMSS
[37]	Below-threshold OPO	55	1064	$LiNbO_3$	SMSS
[21]	Above-threshold OPO	86	1064	KTP	TB
[26, 27]	Below-threshold OPO	55	1080	a-cut KTP	TMSS
[38]	Pulsed squeezing, OPO	37	1064	KTP	TMSS
[39]	Mode-locked OPO	30	1064	KTP	TMSS
[40]	OPO	40	1064	$LiNbO_3$	SMSS
[41]	Pulsed squeezing,OPO	34	1064	$NaNb_5O_{15}$	SMSS
[42]	Sub-threshold OPO	75	from 840 to 790	$KNbO_3$	SMSS
[43]	Pulsed squeezing, OPO	30	1064	KTP	TMSS
[44]	Below threshold OPO	30	1064	KTP	TMSS

(*to be continued on the next page*)

(*continued*)

Refs.	System	Squeezing/%	Wavelength/nm	Medium	Note
[45]	Self-matched LO pulsed squeezing	74	1064	KTP	TMSS
[46]	Pulsed squeezing	12	830	KTP waveguide	SMSS
[47]	Pulsed squeezing	14	1064	$LiNbO_3$ waveguide	SMSS
[48]	Monolithic OPO	72	1064	Mg:$LiNbO_3$	SMSS
[17]	OPA with seeder	58	1064	Mg:$LiNbO_3$	SMSS
[49]	Above-threshold OPO	80	1080	a-cut KTP	TB
[28]	Pulsed squeezing, OPO	28	840	$LiTaO_3$ waveguide	SMSS
[50]	Two type squeezed state	57 or 80	1080	a-cut KTP	TMSS or TB
[22]	Above-threshold OPO	88	1039,1090	a-cut KTP	TB
[18]	OPA with seeder	77	1064	MgO:$LiNbO_3$	SMSS
[51]	Above-threshold	72	1062	KTP	TB
[52]	Monolithic OPA	80	1064	MgO:$LiNbO_3$	SMSS
[53]	Pulsed twin beams	35	1064	KTP	TB
[54]	OPA with seeder	57	1080	a-cut KTP	TMSS
[55]	Above-threshold OPO	74	1080	a-cut KTP	TB
[56]	Portable squeezer source	38 or 74	1080	a-cut KTP	TMSS or TB
[57]	Twin beams in time domain	68	1064	KTP	TB
[58]	Active phase controlled OPO	60	1064	Na:KTP	TB
[59]	OPO and OPA	68	1064	MgO:$LiNbO_3$	SMSS
[60]	Tunable twin beams	50	1041	a-cut KTP	TB
[61]	Self-phase locked OPO	60	1064	PPKTP	TMSS
[24]	Audio frequency squeezing, OPO	72	1064	$LiNbO_3$	SMSS
[62]	Doubled LD pumped OPO	63	1080	a-cut KTP	TB
[63]	Time domain, pulsed squeezing	35	846	$KNbO_3$	SMSS
[64]	Pulse squeezing, OPO	44	846	$KNbO_3$	TMSS
[65]	Pulsed squeezing, OPO	52	1064	PPKTP	SMSS
[66]	Below threshold OPO	40	860	$KNbO_3$	SMSS
[23]	Above threshold OPO	89	1064	KTP	TB
[67]	Below threshold OPO with $\lambda/4$	67	1064	KTP	TMSS
[8]	Above-threshold	40 and 18	1064	KTP	Entanglement
[25]	Doubled LD pumped OPA with seeder	39	1080	a-cut KTP	TMSS
[7]	Active phase controlled OPO	50 and 27	1064	Na:KTP	Entanglement
[68]	Below threshold OPO	80	860	PPKTP	SMSS
[69]	At telecommunication wavelength	30	1535	PPLN waveguide	SMSS
[9]	Above threshold OPO	25 and 13	1080	a-cut KTP	Entanglement
[70]	Below threshold OPO	72	946	PPKTP	SMSS
[71]	Rb D1 line squeezing, OPO	46	795	PPKTP	SMSS
[72]	Squeezing at audio frequency, OPO	60	1064	$LiNbO_3$	SMSS
[73]	Rb D1 line squeezing, OPO	70	795	PPKTP	SMSS
[74]	Cw single passed OPA	33	946	PPLN waveguide	SMSS
[75]	At telecommunication wavelength	52	1535	PPLN waveguide	SMSS
[19]	Below-threshold OPO	87	860	PPKTP	SMSS
[76]	Mesoscopic twin beams	52	632, 778	BBO	TB
[77]	Below threshold OPO	55	1064	PPLN waveguide	SMSS
[78]	Polarization squeezing OPO	56	1064	PPKTP	SMSS
[79]	Low frequency squeezing	55	1064	PPKTP	SMSS
[20]	Below threshold OPO	90	1064	PPKTP	SMSS

Note: SMSS: Single mode squeezed state; TMSS: Two mode squeezed state; TB: Twin beams

forts, which were done by many scientists in the fields of physics and quantum optics, are the understanding and test of fundamental physics and development of a new branch of physics by application of the squeezed state. In earlier years, the applications of squeezed state focused on: The possibility of quantum non-demolition measurements and the improvements in sensitivities of spectroscopic and interferometer measurements. It is the objective for new applications of squeezed state to discover quantum information science—a new branch of physics.

3 Some classical properties of OPO/OPA

As an important device in nonlinear optics, the classical properties of OPO, such as frequency stability, tunability and conversion efficiency, are very attractive as well as in the field of quantum optics. In this section, we discuss some classical properties that are relative to the generation of non-classical state. These properties include the threshold, relaxation oscillation and classical gain.

3.1 Threshold of OPO

To investigate the threshold and relaxation oscillation of OPO, as an example, an NDOPO was introduced in this section. The experimental setup is shown schematically in Fig. 2. The semi-monolithic NDOPO consists of a KTP crystal with a dimension of 3 mm × 3 mm × 10 mm and a spherical output mirror of 20-mm radius, and is carefully designed for the mechanical stability to avoid the surrounding vibrations and acoustic noise. The output mirror is mounted on a piezoelectric transducer (PZT) to adjust the cavity length. One side of the crystal, which is an input mirror, has a multi-dielectric mirror coating of 90 % reflectivity at 532 nm and high reflectivity at 1064 nm, and the other side has an anti-reflection coating at the dual wavelengths. The spherical output mirror has high reflectivity at 532 nm and 95 % reflectivity at 1064 nm. A diode-pumped Nd:YAG laser (Lightwave Electronics, Model 142) served as the pump source of the system. The laser delivered a maximum output power of 400 mW at a fixed wavelength of 532 nm, of which 350 mW was available in front of the OPO. A half-wave plate (P_1) and polarizing beam splitter (PBS_0) were used to adjust the power in front of the OPO. The optical cavity resonates with the pump, the signal and the idler simultaneously, which is a triply resonant OPO. The cavity length is thermally self-locked and the oscillation goes on for more than 40 minutes without active stabilization. The signal and idler beams, which have orthogonal polarizations, are separated by PBS_1. To investigate the relaxation oscillation, the noise of signal beams is measured by a balanced homodyne detector. The detection apparatus is composed of half-wave plate P_2, polarizing beam splitter PBS_2, and two identical high-quantum-efficiency photodiodes (InGaAs; Epitaxx ETX500) matched to equal transcendence low-noise amplifiers. The half-wave plate and the polarizing beam splitter acted to split the beam into two beams with equal intensity. The ac photocurrents of the balanced detector were combined in a hybrid junction to generate sum and difference currents i_1 and i_2, respectively. These currents were inputted to spectrum analyzers that recorded the noise power. The sum signal was a measure of the intensity noise of the beam, whereas the difference signal gave the shot-noise level.

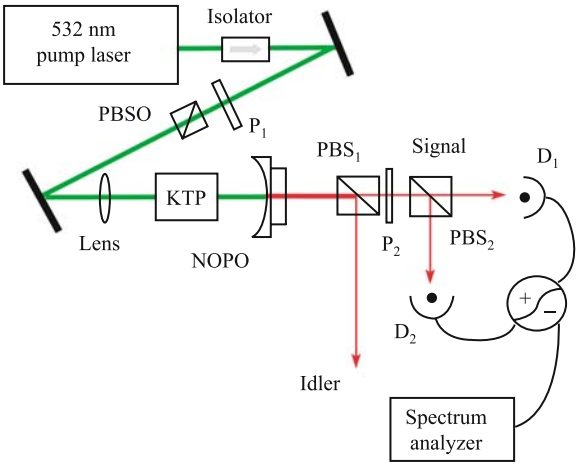

Fig. 2 Experimental setup for a triply resonant cw NDOPO: D_1, D_2, photodiodes; PBS_0-PBS_2, polarizing beam splitters; P_1, half-wave plate for 532 nm; P_2, half-wave plates for 1064 nm.

A calibrated thermal power meter was employed for both the pump-power (P_p) and the output-power (P_out) measurements. Figure 3 shows the results of measurements made over a range of pump powers from 18 to 350 mW. We varied the input power by rotating half-wave plate P_1 of the power adjustment system. In particular, at a pump power of 350 mW an output power of 240 mW was obtained. From these measured powers we computed conversion efficiency $\epsilon = P_\mathrm{out}/P_\mathrm{p}$, obtaining 0.68 ± 0.04 for the frequency down conversion from 532 to 1064 nm. The linear fit is also shown in Fig. 3 (red line), which yields an OPO threshold of $P_\mathrm{th} = 9.0 \pm 1.8$ mW and a slope conversion efficiency of 0.72 ± 0.02. The experimental data was also fitted by a theoretical prediction using the equation of $P_\mathrm{out} = 2\kappa(\sqrt{P_\mathrm{p}P_\mathrm{th}} - P_\mathrm{th})$, where κ

and $P_{\rm th}$ were used as the fit parameters (see blue line). At low pump power (pump powers less than 13 times the pump threshold), the experimental data are very well fitted to the theoretical prediction with fit parameters of $P_{\rm th} = 8.5 \pm 1.3$ mW and $\kappa = 1.2 \pm 0.1$ (see Fig. 3, inset). The fitting threshold is near threshold value of experimental data and from the linear fit of all experimental data. Unfortunately, the output power fell short of the theoretically expected value in the high-pump-power range. In Fig. 3 the output power is higher than the expected value. Possible reasons for this discrepancy include increased sub-harmonic loss and decreased pump loss because of up-conversion, absorption of the OPO fields in the crystal, and thermally induced changes in the crystal's refractive index. All these reasons will induce changes in the pump threshold and in the power slope efficiency and, in turn, in the output power of the OPO. These issues will have to be carefully addressed in the future theoretical mode.

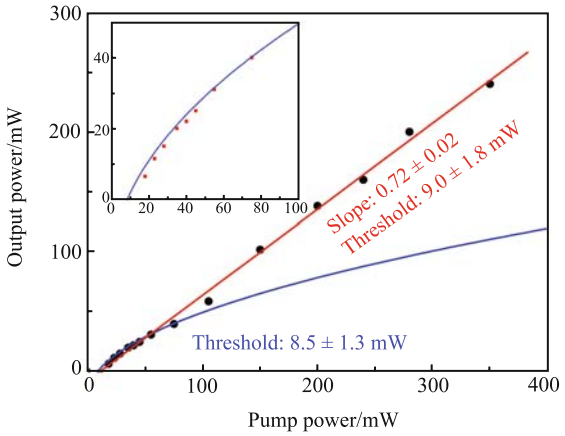

Fig. 3 Output power of OPO measured as a function of pump power. The fit yields an OPO threshold of 8.5 ± 1.3 mW and a slope conversion efficiency of $\epsilon = 0.72 \pm 0.02$.

Note that during each increment of the pump power we observed several axial mode hops of the sub-harmonic wave, which yielded different output powers. Such mode hops are probably induced by absorption of the OPO fields in the crystal. This absorption leads to thermally induced changes in the crystal. The difference in output power can be interpreted as a varying threshold or threshold factor. Reliable operation of the OPO at a chosen threshold factor thus required careful adjustment of the cavity length. For a reproducible measurement of output power versus pump power we fine-tuned the cavity length during cw OPO resonant operation. We did this by applying a manually adjustable offset voltage to the PZT. For each pump-power setting the voltage was adjusted to produce the maximum output power.

3.2 Relaxation oscillation of OPO

It is well known that the intensity noise spectrum of the output single beam of a cw resonant OPO is similar to the noise spectrum of a laser oscillator. Lee *et al.* observed relaxation oscillations in the intensity spectrum of a single beam emitted by an NDOPO pumped by a diode laser [80], and Porzio *et. al.* observed relaxation oscillation in the single-beam spectra of twin beams output from a triply resonant NDOPO for pump power of as much as approximately 15 times the threshold [81, 82]. The relaxation oscillation frequency shifts to higher values as the pump power is increased. The object of investigation of relaxation oscillation is to obtain the noise properties of output from OPO. In theory, it is predicted the intensity noise in the single beam of twin beam will fall down below the shot-noise when the pump power is above four times the oscillation threshold. The detail of indication of squeezing of the single-beam is reported in Ref. [83]. Here we give the relaxation oscillation of our triply resonant NDOPO.

We measured the intensity noise in a single beam of the OPO output by using a balanced homodyne detector to detect a single beam of twin beams (see Fig. 2). Examples of the recorded normalized single-beam intensity noise as a function of noise frequency are shown in Fig. 4 for the OPO operating at pump powers of 12.5, 18, 23, and 28 mW. At high pump powers, the noise spectra were different and clearly showed a broad noise peak with a nonzero center frequency, which is called the relaxation oscillation frequency. This frequency shifts to higher values as the pump power is increased. Figure 5 compares the experimental results (points) with the theoretical values (curve) of the relaxation oscillation frequency obtained based on theory in Ref. [80]. The experimental results fit the theoretical curve very well. The vertical error bars give the uncertainty in determining due to the uncertainty of the oscillation threshold. However, an unpredicted experimental result was observed when the pump threshold factor increased further. Figure 6 shows the normalized intensity noise in a single beam versus frequency for pump powers of 28 to 55 mW. The intensity noise of signal beams decreased with increasing pump power, which is different from the previous case [80−82]. The intensity noise decreased with increasing pump power, indicating the inherent noise character of the single beam generated by an OPO. This behavior is like that predicted by Fabre *et al.* [11] and was recently studied theoretically in detail by Porzio *et al.* [84]. The reduction in the single-beam intensity noise indicates a possibility of using our triply resonant OPO to generate sub-Poissonian light at high pump powers.

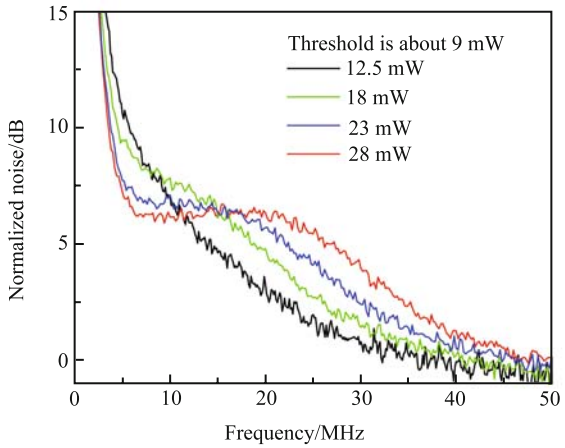

Fig. 4 Normalized single beam noise versus frequency when pump power increases from 12.5 to 28 mW. Resolution bandwidth: 100 kHz, video bandwidth: 100 Hz.

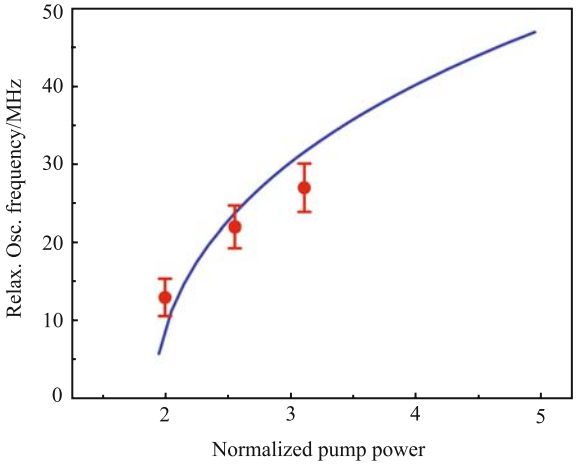

Fig. 5 Measured OPO relaxation oscillation frequency as a function of normalized pump power. The solid curve represents the theoretical predictions, and the dots are the experimental results.

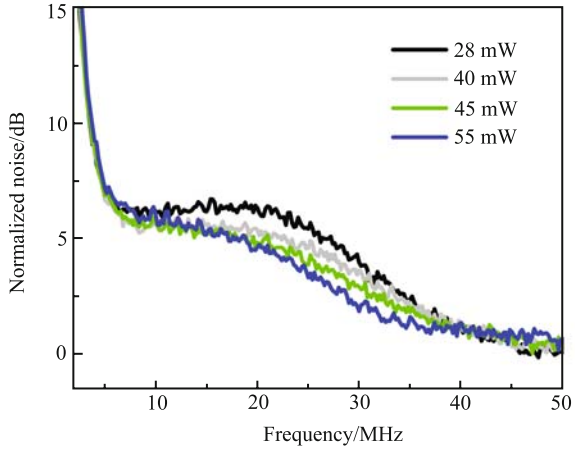

Fig. 6 Normalized single beam noise versus frequency when pump power increases from 28 to 55 mW. Resolution bandwidth: 100 kHz, video bandwidth: 100 Hz.

3.3 Classical gain of OPA

To characterize the OPA, the initial investigation is classical parametric gain. A typical experimental setup of measurement classical gain is shown in Fig. 7. To measure the classical gain, a probe field is introduced to the OPA. The output of the probe field is measured by a scope in the absence and presence of the pump field. The relative phase between the pump and probe fields can be varied by scanning the mirror mounted on the PZT. Experimentally, the classical gain (G) is defined as $G = P_{\rm out}/P_{\rm in}$, where $P_{\rm in}$ and $P_{\rm out}$ are the output powers transmitted by the OPA through the output coupler in the absence and the presence of the pump, respectively. Once the pump power is turned on, the gain depends on the power and the relative phase between the probe and pump waves, i.e., the sign of pump amplitude. So, the OPAs are also phase-sensitive optical amplifiers.

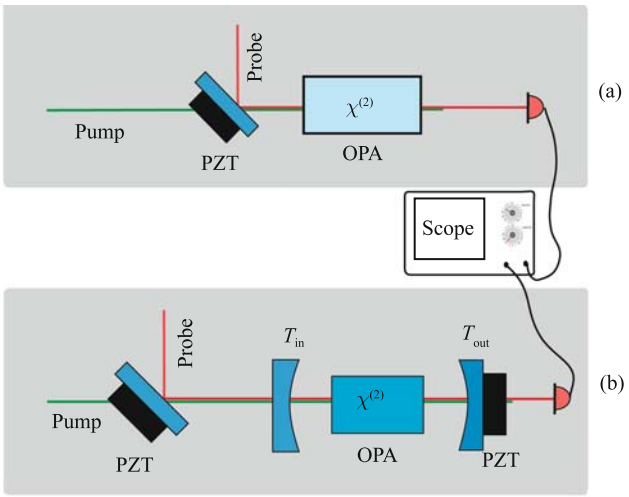

Fig. 7 Experimental setup for measurement parametric classical gain. **(a)** Single pass through OPA. **(b)** Cavity enhanced OPA.

For the devices, which are pumped by laser pulses [see Fig. 7 (a)], a typical measurement of phase sensitive amplification of OPA is shown in Fig. 8 (a). When the pump is on and the phase of the probe light relative to the pump light is scanned, the output probe signal fluctuates due to the changes of the relative phase. The amplification gain ($G_{\rm A}$) and deamplification gain ($G_{\rm D}$) is defined as the maximal probe power and minimum probe power when pump is on divided by probe power when pump is off, respectively. The observed maximum amplification gain and minimum deamplification gain are also shown as a function of the pump average power in Fig. 8 (b). As shown in the figure, in this experiment, a minimum deamplification of -5.7 dB and maximum amplification of 10 dB were obtained at the provided

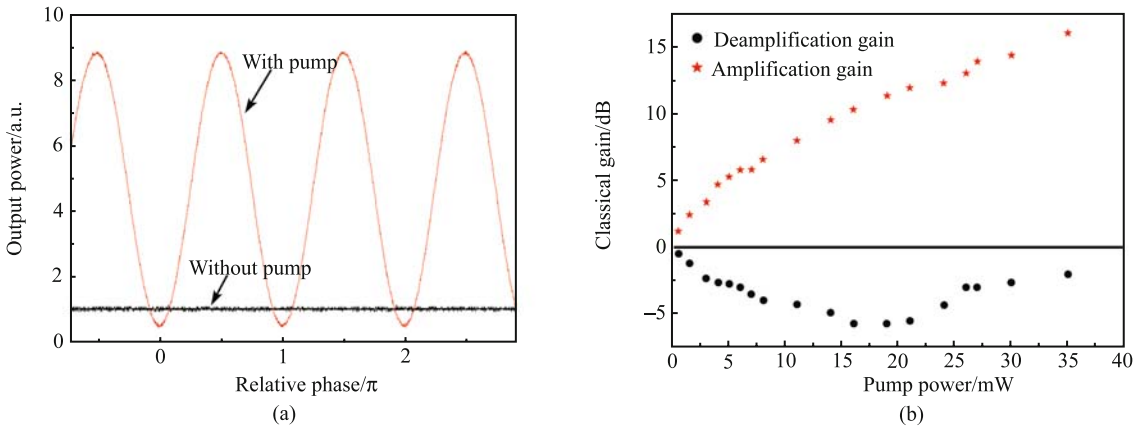

Fig. 8 A typical measured result of classical gain for a single pass through OPA. **(a)** Output probe versus the relative phase between the input probe and pump beams. **(b)** Classical parametric gain versus average pump power.

pump power of about 20 mW. With further increase of the pump power, the amplification gain can be monotonously increased; however, the deamplification gain starts to increase instead decreasing. It seems that the deamplification of the input beam becomes impossible at high pump powers. In the perfect case, the product of amplification gain and deamplification gain should be unity; however, the product deviates from unity as the pump power increases as shown in Fig. 8 (b). Note the deamplification gain is always less than the amplification gain. A similar disparity between the amplification and deamplification response of an OPA was reported in many experiments on the generation of pulsed squeezed state using bulk crystal and the lack of deamplification is due to the phenomenon of gain induced diffraction, which only occurs at high pump power.

Because of the existence of enhanced cavity, the classical gain of an enhanced OPA is complex than that of single-pass through OPA. If the probe wave of power $P_{\rm probe}$ is on resonance with the cavity [see Fig. 7 (b)], then $P_{\rm in} = 4P_{\rm probe}T_{\rm out}T_{\rm in}/(T_{\rm out}+T_{\rm in}+A)^2$, where A is the intracavity loss of the OPA cavity and $T_{\rm in}$ ($T_{\rm out}$) is the transmission of the input(output) coupler, the output power transmitted by the OPA cavity in absence of the pump. Once the pump is turned on, the output power $GP_{\rm in}$ has a gain G which depends on the power of pump field and the phase between the pump and probe fields. Figure 9 shows the calculated results of the OPA [85]. We note that at close to the threshold, the amplification gain ($G_{\rm A}$) obtained from the transmitted beam can be very large. However, the deamplification gain ($G_{\rm D}$) limit at threshold is 1/4. In fact, the strongest deamplification factor is given as $G_{\rm D} = 1/(1+\sqrt{P_{\rm p}/P_{\rm th}})^2$, which closes 1/4 at the input power of the threshold independent of the employed resonator and the power of the probe field. The agreement of this expression with the experimentally measured $G_{\rm D}$ was observed by many researchers. On the other hand, the maximum amplification depends on the probe power since it is limited by the depletion of the pump. Both the calculated and experimental results show that the maximum amplification gain was obtained at the seed power that is as low as possible. In addition, the maximum amplification gain also depends on the employed resonator. The calculated results clearly show that it is strongly dependent on the escape efficiency of $\xi = T_{\rm out}/(T_{\rm out}+T_{\rm in}+A)$ when the pump approaches the threshold. In experiment, maximum classical gains of 10 000 and 3 260 were observed employing OPAs with 0.96 and 0.88 escape efficiencies, respectively [52, 86]. An empirical expression of amplification gain is given as $G_{\rm A} = (4\xi P_{\rm th}/P_{\rm in})^{2/3}$. Note, however, that this gain factor cannot be directly used for signal amplification, because the injection of the seed wave through the input port (HR mirror) leads to high losses. Figure 10 shows an observed experimental classical gain of the OPA when

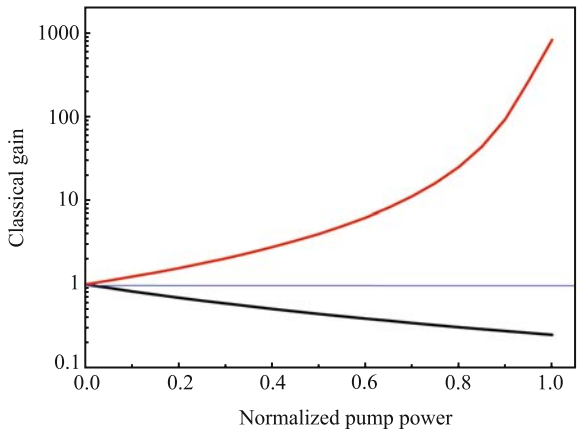

Fig. 9 Calculated classical gain of the cavity enhanced OPA. The gain is calculated by considering the ratio of transmitted powers with OPA pump power on and off.

a cw laser is employed as light source. To observe the classical gain of OPA, the transmitted power of an enhanced cavity is recorded by an oscilloscope when the enhanced cavity is scanned. The classical amplification (deamplification) gain (G) is simply calculated by transmitted maximal (minimum) power when the pump is on divided by transmitted power when the pump is off. In Fig. 10, an amplification gain of about 3 and deamplification gain of about 0.8 were obtained.

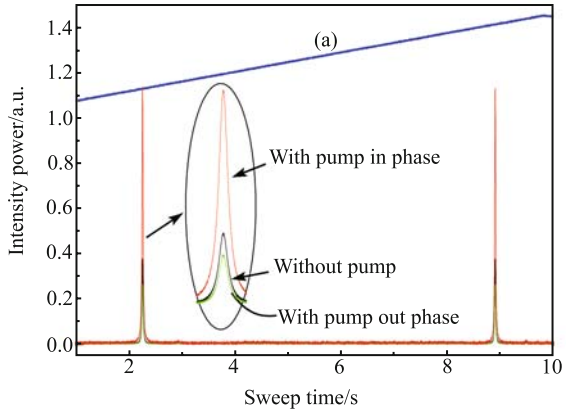

Fig. 10 A typical measured result of classical gain for a cavity enhanced OPA. The OPA is electro-optically modulated by application of a ramp voltage as shown in trace (a). The black trace shows the small input signal beam injected at the input coupler of the OPA. With the pump field of OPA turned on, the red trace and green trace shows the transmitted amplified and deamplified output when the pump field is in phase or out phase with the signal field.

From the above discussion, we should note that in experiment, to evaluate the parametric amplification process, the amplification gain is always measured when the cw laser is used as light source because the deamplification gain is limited to 0.25 independent on the employed cavity; however, the deamplification gain is measured when the pulse laser is utilized as light source. In practical experiments of generation of pulsed squeezed state, the deamplification gain is restricted when the amplification gain keeps increasing.

4 Generation of squeezed state from OPA

In this section, two experiments on the generation of squeezed state are presented. One is generated single mode squeezed state from a single-pass through OPA, which is pumped by pico-second pulses. Another is generated two-mode squeezed state from an enhanced cavity, which is pumped by amplified and noise suppressed frequency doubled laser diode.

4.1 Single mode squeezed state

The experimental scheme of the generation of single mode squeezed state is presented in Fig. 11. The initial pulses are obtained from a cw mode-locked Nd:YVO_4(VAN) laser, which is pumped by a semiconductor laser diode, operating at 1064 nm with a duration of 7 ps and a pulse repetition rate of 76 MHz. This laser system provided an average power of about 750 mW. The fundamental was divided into three parts. A major fraction of this light was sent to a single pass through SHG system to generate an efficient 532 nm pump source for pumping the OPAs. In our SHG system, a 5-mm-long, 2-mm-wide, and 1-mm-thick dual-band antireflection-coated periodically poled potassium titanyl phosphate (PPKTP) crystal is used as a nonlinear material. The crystal is set inside a homemade oven, in which the temperature is actively controlled around the temperature for achieving maximum SHG output. An electronic feedback circuit is employed to actively stabilize the temperature fluctuation of crystal to ± 0.01 °C. In particular, about 300 mW of green light was produced when the fundamental input power is about 700 mW. However, in the following experiments, about 50 mW of green light is employed to pump the OPA. Because of the high nonlinear coefficient of PPKTP, more than 40 % SHG efficiency was obtained.

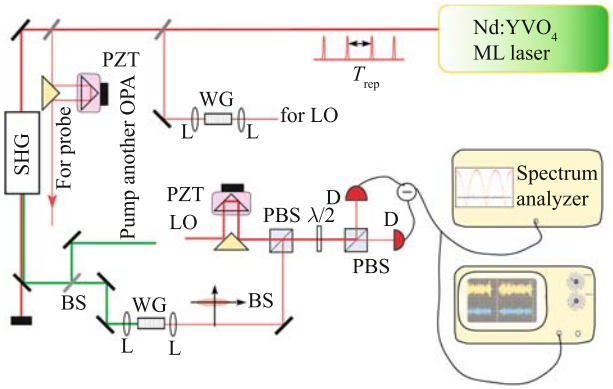

Fig. 11 Experimental setup. SHG: second harmonic generator, WG: waveguide, BS: 50:50 beam splitter, L: lens, PBS: polarizing beam splitter, Ds: photodiodes, PZTs: piezoelectric transducers, $\lambda/2$: half-wave plate, and LO: local oscillator.

The nonlinear material for the generation of squeezing states in our experiment is a single-mode PPLN waveguide (WG) with a length of 5.0-mm and effective core area of 3 μm × 5 μm. The choice for a single-mode PPLN waveguide has the benefit of the transverse confinement and of the possibility of spatial mode control. In bulk crystals, several problems hamper the available gain. Two phase quadrature of the signal field experi-

ence different spatially dependent gains, leading to the introduction of additional modes along with an accompanying loss of squeezing the phenomenon of gain-induced diffraction. In a waveguide, the transverse profile is determined largely by the step-index changes rather than by nonlinear optical index changes, so the mode can be controlled. This leads to more efficient nonlinear interaction between the pump and signal fields and also produces a squeezed field in a well-defined spatial mode. After the generated second harmonic light exited the SHG system, we separate the second harmonic from the fundamental wave. The pump lights are carefully focused into the OPA (WG) with a lens. The down-conversion signal produced in the OPA and LO with orthogonal polarization are mixed at the first polarizing beam splitter (PBS), and propagate collinearly to the balanced homodyne detector. A half wave plate is inserted to rotate the beam polarization to 45° and another PBS split it into two equal beams. The output of the homodyne detector can be monitored by a spectrum analyzer in the frequency domain or be recorded by a digital oscilloscope, which records and analyzes the information in the time domain.

To observe a high degree of quadrature squeezing, we believe it is very important to achieve a LO that matches the generated squeezed vacuum very well. Contrary to the previously reported use of the remaining 1064 nm light from the SHG system, in which the temporal envelope is greatly changed from that of the fundamental wave [75], the LO pulses are obtained by splitting a small portion of the laser emission. The intensity and polarization of this beam are adjusted with a set of half-wave plates and polarizers (not shown in Figure). The LO is then put through a similar PPLN waveguide to ensure proper spatial mode matching to the signal. Before the mixing at PBS, the LO delayed temporally to ensure simultaneous arrival with the signal pulse and the phase of LO can be varied by scanning a prism mounted on a piezoelectric translator (PZT).

Another small fraction (about 2 mW) of the fundamental beam is taken out to serve as a probe to study classical parametric amplification occurring in the OPA. Once again, the probe is also delayed temporally to ensure simultaneous arrival of the OPA with pump pulses and the phase of probe light relative to the pump light is varied by scanning the prism mounted on a PZT.

To evaluate the OPA, the first step is to investigate the classical parametric gain. In this run, both the probe and pump was injected to the OPA. A minimum deamplification of -5.7 dB and maximum amplification of 10 dB were obtained at the pump power of 20 mW. The phase sensitive OPA can be exploited for the generation of squeezed vacuum state of light. In this run, the OPA was only pumped by the pump light and the probe signal input was blocked. The generated squeezed vacuum from OPA is mixed with LO beams at PBS and measured by the homodyne system. The output of the homodyne detector is recorded using a spectrum analyzer. The squeezing at a fixed analyzing frequency of 10 MHz is shown in Fig. 12. It was obtained by recording the output of the homodyne detector with the spectrum analyzer when scanning the phase of the LO. The power of the pump light is fixed at 20 mW, at which minimum deamplification gain is obtained. The analyzing frequency of spectrum analyzer is set at center frequency of 10 MHz and span of 0 Hz. The noise level of the vacuum (SNL) is normalized to 0 dB and the electronic noise of homodyne is subtracted. The normalized phase sensitive noise shows 3.4 dB squeezing below the SNL and antisqueezing of 13 dB.

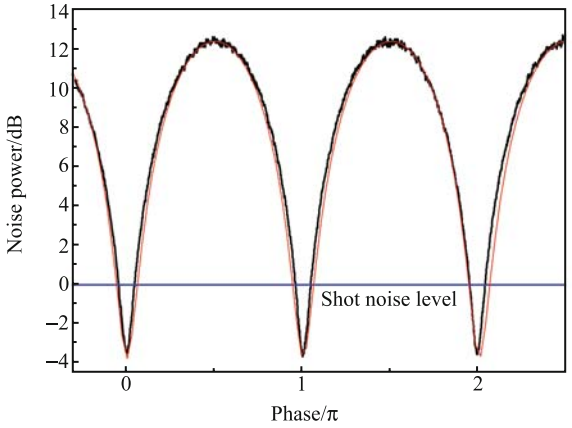

Fig. 12 Normalized noise power of squeezed vacuum at fixed analyzer frequency of 10 MHz. The black curve is measured result and the red dashed curve is a fitted result using parameters, which are calculated from the classical amplification and deamplification gain. Resolution bandwidth is 300 kHz and video bandwidth is 100 Hz.

We also measured the squeezing state in the time domain. In this run, the output of the homodyne detector is recorded by a digital oscilloscope. In our experiment, a scope provided with an analog bandwidth of 4 GHz, a sampling rate of 5 GSamples/s, and a storage depth of 500 000 points, is employed. In the time domain, one value of field quadrature is yielded by one laser pulse. It was realized by integrating the output of the homodyne detector over the pulse duration time. In our case, we numerically integrated a time sequence of 500 000 samples, covering time windows of 100 μs and including 7600 pulses each over a time interval of length $T = 13$ ns, corresponding to 66 points, to produce measurements of all the pulses in the sequence and perform statistics.

Figure 13 gives the measured quadrature amplitude distribution and the best fitting Gaussian distribution for squeezed quadrature, antisqueezed quadrature and SNL. The quadrature amplitude distributions are constructed from 7600 pulses at corresponding LO phase, which is monitored by a spectrum analyzer and measured in the frequency domain. The measured results both in frequency domain and in the time domain show a squeezing of −2.3 dB below the shot noise level and antisqueezing of 7.5 dB above the SNL.

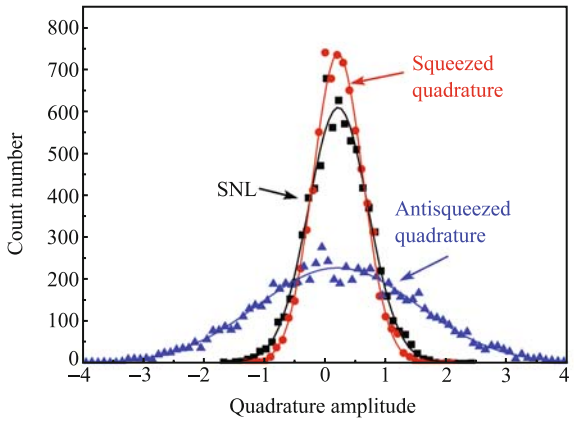

Fig. 13 Measured quadrature amplitude for squeezed quadrature, antisqueezed quadrature and shot noise level in time domain.

In the absence of perfect detection efficiency, the squeezing is degraded with the overall detection efficiency. Quantum efficiency of photodiode, transmission of optical components and mode matching between the LO and signal can be accounted for by the detection efficiency $\eta_{\rm d}$. A further consideration is mis-mode-matching ($\eta_{\rm m}$) between the probe and pump light because it also introduces noise to the OPA system. Therefore, an overall efficiency η, which is determined by detection efficiency and mode-matching efficiency, is given by $\eta = \eta_{\rm d}\eta_{\rm m}$. A phenomenological expression for the measured noise power can be expressed by

$$P_N(\phi) = \eta(\mathrm{e}^{2r}\cos^2\phi + \mathrm{e}^{-2r}\sin^2\phi) + 1 - \eta \qquad (1)$$

where ϕ is the relative phase of LO and r is the squeezing parameter. By fitting this formula to the experimental squeezing results, we can extract the squeezing parameter r and overall detection efficiency η. The dashed curve in Fig. 12 is a theoretical fit to the data where fitted parameter values are $r = 1.67$ and $\eta = 0.6$. Furthermore, the mis-mode matching parameter ($\eta_{\rm m}$) and squeezing parameter (r) were also able to fit from the classical parametric gain using the equations

$$\begin{cases} G_{\rm A} = \eta_{\rm m}\mathrm{e}^{2r} + 1 - \eta_{\rm m} \\ G_{\rm D} = \eta_{\rm m}\mathrm{e}^{-2r} + 1 - \eta_{\rm m} \end{cases} \qquad (2)$$

where e^{2r} and e^{-2r} are the intrinsic parametric amplification gain and deamplification gain. Taking into account a detector quantum efficiency of 0.85, the waveguide loss of 1 dB/cm and the total propagation loss of 3 %, we obtained a total detection efficiency ($\eta_{\rm d}$) of 0.73. The fitted value of r and $\eta_{\rm m}$ are in good agreement with the estimated values from the parametric gain and amount of measured squeezing at a pump power of about 20 mW.

4.2 Two-mode squeezed state using LD as light source

The experimental setup for the generation of two-mode squeezed state is shown schematically in Fig. 14. A grating-stabilized single-mode extended-cavity diode laser (ECDL) serves as the primary light source. The wavelength of the diode laser is selected at 1080 nm in our experiment since it can realize non-critical phase matching in an a-cut KTP. The master laser provides 50 mW of power after the grating, and more than 30 mW is available for injection into the tapered amplifier chip. The output power from the amplifier chip is about 450 mW. To reduce the excess noise of the diode laser, we sent the beam through a filter cavity and used the resonant optical feedback. A small fraction of the transmitted light was picked off by the polarizing beam splitter (PBS) with a half wave plate, which can also control the optical feedback level, and sent into ECDL as a resonant optical feedback. When the cavity is locked, we measured more than 200 mW transmitted light power for an incident power of 380 mW, representing a transmission efficiency of 53 %. The intensity noise at particular power level (approx. 20 mW) of the laser light is measured and it is shot noise level at 15 MHz, hence transferring no classical noise into the second harmonic and seed at frequencies higher than 15 MHz. The details of noise suppression of the amplified diode laser were reported in Ref. [87]. Most of the noise suppressed laser power is introduced

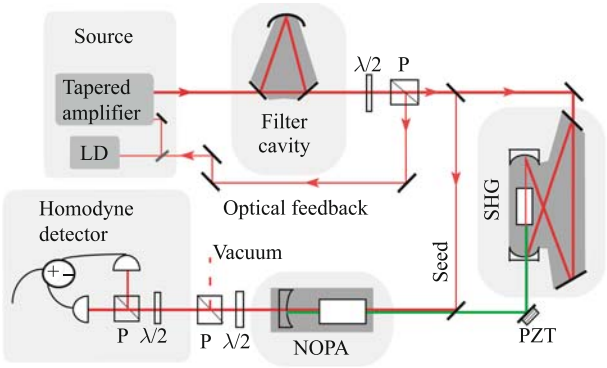

Fig. 14 Experimental setup. SHG: second harmonic generator; NOPA: nondegenerate optical parametric amplifier; $\lambda/2$: half wave plate; BS: beam splitter; P: polarizing beam splitter.

into the frequency doubler to generate a second harmonic at 540 nm as pump beam for the NOPA. About 5 mW of power is injected to the NOPA as a seed wave. The polarization of the seed wave is 45° relative to the b axis of the KTP crystal, and it is decomposed to signal and idler seed waves with identical intensity and the orthogonal polarizations along the b and c axes, respectively, which correspond to the vertical and horizontal polarization. The generated bright two-mode squeezed state is detected by a homodyne detector.

The NOPA has a semimonolithic configuration consisting of a concave mirror of 20-mm radius of curvature coated with a $T_{\rm out} = 2$ % transmission for 1080 nm and high reflection for 540 nm. It serves as an output coupler for our NOPA. A facet of KTP inside the cavity was coated for antireflection at both 1080 and 540 nm. The other facet was coated for antireflection at 540 nm and high reflection at 1080 nm. It acts as the input mirror of the pump field at 540 nm. The measured finesse of the resonator is 300, the free spectral range is 6 GHz, and the cavity bandwidth is $\gamma = 20$ MHz. We calculated a total round-trip loss $L_{\rm NOPA} = 0.3$ % by the measured finesse. The escape efficiency of $\eta_{\rm e} = T_{\rm out}/(T_{\rm out} + L_{\rm NOPA}) = 0.87$ is obtained. Due to the large transmission of input coupler at 540 nm, the pump field only passes the cavity twice without resonating. The crystal nonlinear efficiency of $E_{\rm NL} = 1.1 \times 10^{-3}{\rm W}^{-1}$ was estimated from the SHG process. From this we deduce an expected threshold pump power for parametric oscillation, $P_{\rm th} = (T_{\rm out} + L_{\rm NOPA})^2/4E_{\rm NL} = 120$ mW.

The principal difficulty of the NOPA resides in frequency-degenerate operation. There are several ways to solve this problem, such as seed injection, inserting a half-wave plate in cavity, and active adding phase-locking between the signal and idler. For this purpose, the seed wave is injected in our work. The NOPA cavity must be simultaneously resonant at the signal and idler of seed beam frequency. By fine tuning the crystal temperature, the birefringence between the signal and idler waves in KTP is compensated and the simultaneous resonance is obtained. Once the double resonance is completed, phase sensitive parametric amplification/deamplification was realized. Operating below threshold and scanning the pump phase with the PZT, one observes maximum amplification factors up to 20. Stable operation of the squeezer can be achieved by locking the cavity on the frequency of the seed wave via a dither-locking technique.

It has been demonstrated that the orthogonally polarized modes, which are produced from the projection of the output signal and idler mode along direction at ±45° relative to the sign beam polarization, have squeezed fluctuations [88]. Different from previous work [23, 54], where the squeezed vacuum is measured by introducing local oscillator light, we directly measured the squeezing of the bright two-mode from the NOPA. The signal and idler modes superposed by a rotating half-wave plate at an angle of 22.5° relative to the signal beam polarization, and then the coupled modes were separated by the polarizing beam splitter. The noise of the bright mode is measured by the self-homodyne detection system. The ac photocurrents of the detector are combined in a hybrid junction to generate the difference and sum currents i_- and i_+, which indicated the shot noise reference and the intensity noise levels, respectively.

Figure 15 shows the measured variances at $\omega = 16$ MHz when the pump power was about 100 mW. Trace (b) and (c) refer to the amplitude noise and the shot noise limit, respectively, when the pump phase is fixed on deamplification operation. A measurement of $V_{\rm det}(i_+)$ and $V_{\rm det}(i_-)$ is also given in traces (f) and (e) when the phase is scanned. The amplitude squeezing up to 2.1 ± 0.2 dB is measured under the total detection efficiency of $\eta_{\rm d} = 86$ % (detector quantum efficiency 90 % and propagation efficiency 96 %). Trace (d) gives the measured shot noise limit without pump and trace (a) gives the electronic noise of our detector. We note that the noise powers for the available light power is close to that of the electronic noise floor, so the electronic noise floor should be subtracted. The inferred value after taking into account the electronics floor is 2.5 ± 0.2 dB. In a simplified mode the detected amplitude variance depends not only the component of squeezing(V_-) but also the component of antisqueezing (V_+) and is expressed by [17]

$$V_{\rm det}(\omega, \phi) = V_- \cos^2\phi + V_+ \sin^2\phi \qquad (3)$$

where

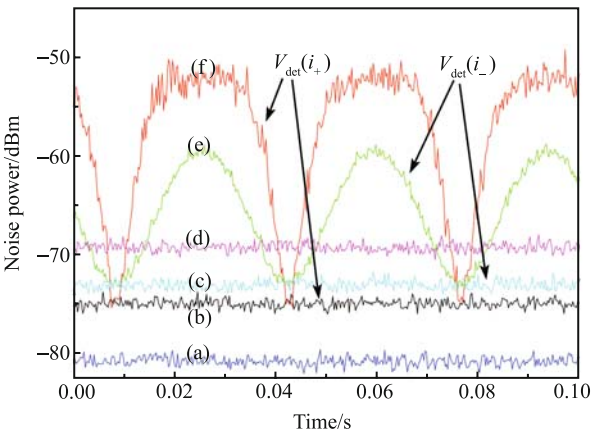

Fig. 15 Noise power of i_+ and i_- generated at the homodyne detector. Measured frequency, 16 MHz; resolution bandwidth, 300 kHz; video bandwidth, 3 kHz. For details see text.

$$V_{\pm}(\omega) = 1 \pm \eta_{\rm d}\eta_{\rm e}\frac{4\sqrt{P_{\rm p}/P_{\rm th}}}{(1 \mp \sqrt{P_{\rm p}/P_{\rm th}})^2 + (2\omega/\gamma)^2}$$

Using the parameters of our experiment indicated in the preceding paragraphs, a theoretical squeezing of 2.5 dB is predicted. The experiment results are very well in agreement with this prediction. Although the squeezing of just 2.1 dB is observed, it is the first experiment on generating squeezed state directly using LD as a light source.

From Eqs. (3) and (4), we know the squeezing degree depends on many factors. To improve the amount of squeezing, each of factor has to be improved. Here we discuss each limiting factor in detail.

Escape efficiency ($\eta_{\rm e}$) Escape efficiency is the main factor for the generation of squeezed state from OPO/OPA. The escape efficiency of the OPO is the ratio of output coupling transmission to the total cavity losses given by $\eta_{\rm e} = T_{\rm out}/T_{\rm total}$. Obviously, the escape efficiency can be increased by reducing the intracavity losses or increasing the transmission of the output coupler. The former depends on the amount of optical components of the cavity, the technique of the film coating and the quantity of the nonlinear crystal. The monolithic OPA configuration has the minimum intracavity losses. We can also improve the escape efficiency by increasing the transmission of the output coupler at the expense of a much larger OPO threshold. Hence, further increase in the escape efficiency is only feasible with a more powerful laser source. Now, because of the polishing and coating techniques in experiments, it is not difficult to achieve an escape efficiency of more than 0.95.

Detection efficiency ($\eta_{\rm d}$) Detection efficiency consists of two factors. One is the quantum efficiency of photodiodes and the other is the homodyne efficiency or visibility between the LO and probe light of the squeezed state. With the use of the spatial mode cleaner, the homodyne efficiency of the OPO system can reach a level of 0.98. The quantum efficiency of the photodiodes is limited by the maker. Although quantum efficiency of more than 0.99 of Si photodiodes was reported, it only worked on the special wavelength. In usual experiments, a quantum efficiency of photodiodes is around 0.9.

Cavity linewidth (γ) To observe a larger amount of squeezing, a larger linewidth (γ) is desirable. The best squeezing is only able to observe when the analyzing frequency (ω) can be negligible compared with the cavity linewidth. Another advantage of broadening of the OPO cavity linewidth is increasing the escape efficiency.

Threshold power ($P_{\rm th}$) From Eqs. (3) and (4), we note that the amount of vacuum squeezing has only a square-root dependence on the pump power of the OPO. Hence, this factor is not crucial. In fact, the best vacuum squeezing results from OPO were obtained at a level sign if scantly lower than the OPO threshold because of the phase stability of the system.

Phase fluctuation ($\delta\phi$) Phase fluctuation becomes more and more acute with larger squeezing. The vibration of the reflecting surfaces introduce phase fluctuation in the relative phase of the LO and the squeezed beam. If these vibrations are faster than the time required for the spectrum analyzer to gather a single pixel of information, then that point will not be a pure measurement of the noise at phase angle of ϕ in Eq. (3). Instead, it will be a measurement of the noise integrated over some range of angles $\phi \pm \delta\phi$. If this happens, then some of the noise from the antisqueezing quadrature is coupled into what was intended to be a measurement of the squeezed quadrature. This will reduce the amount of squeezing that can be observed, since generating larger amount of squeezing usually accompanies producing a larger amount of antisqueezing at the same time. Recently, it has been addressed that more than 10 dB squeezing can be observed only at the condition of the phase fluctuation $\delta\phi$ less than 1.5°. This is a challenging factor with the present technology to observe the larger amount of squeezing in experiment.

5 Generation of twin beams from NDOPO

Twin beams is another non-classical state generated by NDOPO operating above its threshold. In this section, we give an example of generating twin beams from NDOPO. The experimental setup is shown schematically in Fig. 16. The NDOPO setup is the same pump-enhanced signal and idler resonant semimonolithic OPO used in Section 4 to investigate the threshold and relaxation oscillation. Twin beams were produced when the OPO is operating above the threshold. The twin beams are measured either in the frequency domain or in the time domain. In the frequency domain, the twin beams, which have orthogonal polarizations, are first separated by a PBS and then detected with two high efficiency photodiodes. The photocurrents are amplified by carefully balanced, low-noise amplifier. In our experiment, the power imbalance between the two beams is less than 3 %. Noise spectrum of the subtracted photocurrent is monitored by a spectrum analyzer. The shot-noise level is measured by rotating the half wave plate ($\lambda/2$) by 22.5 degrees relative to the PBS axis. Since the signal and idler beams are mixed, quantum correlation between the two arms is destroyed. This shot noise level can also be confirmed by injecting a laser beam onto another port

of the PBS.

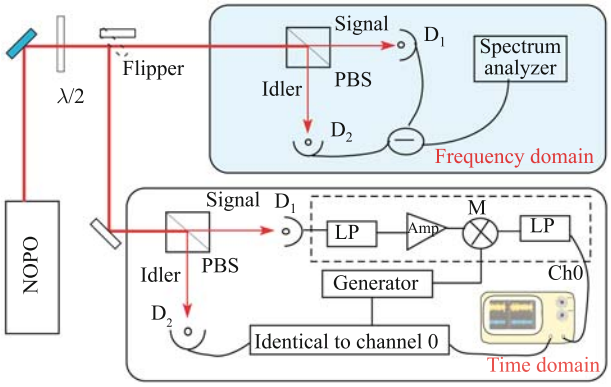

Fig. 16 A schematic of the experimental setup. NDOPO: Nondegenerate optical parametric oscillator, λ/2: half-wave plate, PBS: polarizing beam splitter, D_1, D_2: detectors, LP: low-pass filters, Amp: low-noise electronic amplifier, M: mixer, Ch: channel.

On the other hand, in the time domain, the orthogonally polarized twin beams emitted by the NDOPO are detected separately by two highly efficient detectors. Because the photon fluxes are high, the detectors do not resolve individual photons but generate large average currents with small fluctuations as a result of any (quantum and classical) fluctuations of the waves. After it passes through a 21.4-MHz low-pass f filter, the photocurrent is amplified by a low-noise 46-dB-gain amplifier. Rather than measuring currents $i_s(t)$ and $i_i(t)$ directly, for technical reasons we measured their spectral components $i_s(\Omega, t)$, and $i_i(\Omega, t)$ in a small bandwidth about rf $\Omega = 4$ MHz, where we obtained the best intensity difference squeezing by mixing currents $i_s(t)$ and $i_i(t)$ with rf local oscillators of frequency Ω. The near-dc-region down converted frequency outputs of the mixers are further amplified and low-pass filtered. Their fluctuations are detected within the bandwidth of 100 kHz through the low-pass filters. The data of the fluctuations can be recorded by a computer or a digital oscilloscope, and we obtained all quantum characterization of twin beams by analyzing the recorded data.

The measured intensity difference spectrum of the twin beams, which is generated by a nondegenerate OPO, is expressed as

$$S(\omega) = 1 - \frac{\eta_e \eta_d}{1 + (\omega/\gamma)^2} \quad (5)$$

where ω is the analysis frequency, γ is the cavity linewidth, η_e is the escape efficiency and η_d is the detection efficiency. In this experiment, a total detection efficiency (η_d) of about 90 % is obtained. The detection efficiencies in our experiment were measured with ∼92 % photodetector quantum efficiency and ∼98 % propagation efficiency.

Figure 17 shows the best intensity difference noise reduction of the twin beams generated by our OPO with output coupler transmissions of 5 % and 8.5 %, respectively. The analysis frequency range in the figure is from 1 to 20 MHz. The maximum noise reduction was 7.2±0.3 dB (80 %) below the shot-noise limit at an analysis frequency of 3 MHz by the OPO with 5 % transmission of output coupler. The total output power of ∼26 mW (13 mW per beam) was obtained when the pump power was ∼40 mW (approximately four times the threshold). The values predicted by Eq. (5) (solid curve) with the experimentally measured parameters (η_e, η_d, and γ) are shown for comparison. The experimental results agree with the theory very well. The total loss of T_{total} =5.5 % for the OPO with 5 % transmissions of output coupler is estimated by measuring the finesse of the cavity and escape efficiency of $\eta_e = T_{out}/T_{total} = 0.9$ is obtained. The escape efficiency can be further increased by use of an output coupler with transmission of 8.5 %. Since we only replace the output coupler, we believe that the significant change of the intracavity losses does not occur. Hence, the escape efficiency can be improved to $\eta_e = 0.95$ with the output coupler of transmission of 8.5 %. With this OPO, an intensity difference squeezing of 8.6 dB was obtained. Another advantage of larger escape efficiency OPO is the broadening of the OPO cavity linewidth. We can see that the intensity difference squeezing stays at the level of 8.0 dB even at the analysis frequency of 20 MHz.

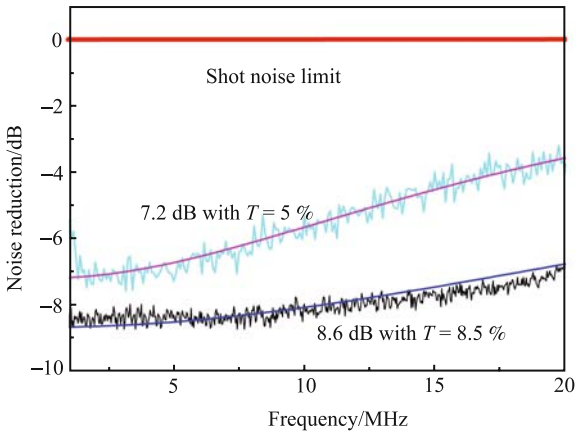

Fig. 17 Intensity difference noise reduction versus frequency. Resolution bandwidth, 100 kHz; video bandwidth, 100 Hz.

The experimentally measured result in the time domain is shown in Fig. 18. It is a direct representation of the correlation between the noise currents of beams 1 and 2 for coherent light and twin beams rotated by 45° and 0° as recorded using a digital oscilloscope. The

total number of data points of each color was 200 000. Each point corresponded to one simultaneous measurement of beams 1 and 2. To show the quantum character of the measured distribution, after the data were stored, we sampled the variances and probability distributions. The variances are listed in Table 2. Note that the variance of difference between channels 0 and 1 is approximately twice that of channel 0 or channel 1 for the coherent light. This result satisfies the property of normal random numbers. The difference variance of the twin beams when they are rotated by 45° has the same value as the difference variance of the coherent light. This result proved that we could also record the shot-noise level when the twin beams were rotated by an angle of 45°. To quantify the amount of measured non-classical correlation between the twin beams, we determined the photon-number difference noise normalized to the shot-noise level $F = Var^{0^\circ}(\mathrm{Ch0} - \mathrm{Ch1})/Var^{45^\circ}(\mathrm{Ch0} - \mathrm{Ch1})$, where ch means channel, over the recorded data. We obtained $F = -4.9$ dB (0.32-fold noise suppression) in this measurement.

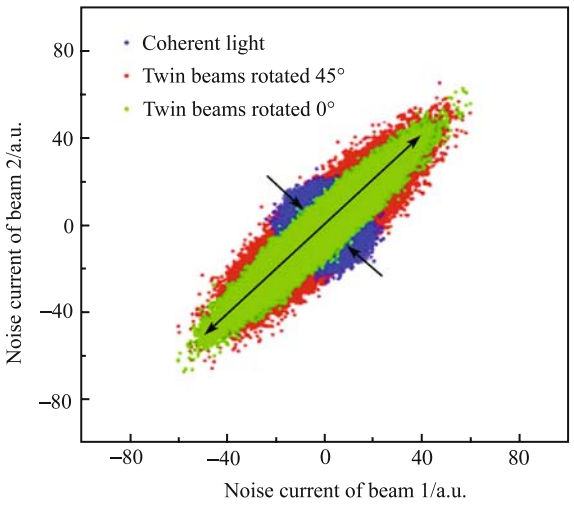

Fig. 18 Correlation between the noise currents of beams 1 and 2 at 4 MHz.

Table 2 Measured variance of twin beams and coherent light.

	Coherent light			Twin bems					
				Rotated 45°			Rotated 0°		
Ch No.	0	1	0−1	0	1	0−1	0	1	0−1
Var.	30.1	32.0	58.8	182.8	198.5	58.5	183.1	198.0	19.0

6 Generation of entanglement state from OPO/OPA

An entangled state can be generated either directly by type II NDOPA/O or by combining at a beam splitter two independently squeezed fields produced via two type I DOPAs. This observation is the extension of the fact that a two-mode squeezed state is equivalent to two single-mode squeezed states combined at a 50:50 beam splitter. Type I DOPAs produce only a single squeezed field, rather than a two-mode squeezed field, so that double resources are required. However, such systems have significant benefits in terms of stability and controllability. Improvements have been made not only in the strength and stability of the interaction, but in the frequency tunability of the output fields and in overall efficiency. Usually, the level of squeezing of 6 dB and the stable operation of several hours can be achieved to date. Furthermore, the pulsed single mode squeezed state can be produced by employing a single pass pulsed configuration OPA. The frequency bandwidth of the squeezed state can reach the order of some THz. On the other hand, the multi-colored entangled state can only be produced from above a threshold type II NDOPO.

6.1 Generation of the entanglement by combining two squeezed states

First of all, let us see the generation of entanglement by combining two squeezed vacua with the scheme shown in the shadow part of Fig. 19. The two output beams A and B have entanglement or EPR correlation of the type originally discussed by Einstein, Podolsky, and Rosen by interference two squeezed vacua ($\hat{a}_1$, $\hat{a}_2$). The figure illustrates this interference and the stick-ball figures graphically show the interference in a phase space representation. Squeezed vacua ($\hat{a}_1$, $\hat{a}_2$) are expressed as

$$\begin{aligned} \hat{a}_1 &= \mathrm{e}^{r}\hat{x}_1^{(0)} + \mathrm{i}\mathrm{e}^{-r}\hat{p}_1^{(0)} \\ \hat{a}_2 &= \mathrm{e}^{-r}\hat{x}_2^{(0)} + \mathrm{i}\mathrm{e}^{r}\hat{p}_2^{(0)} \end{aligned} \tag{6}$$

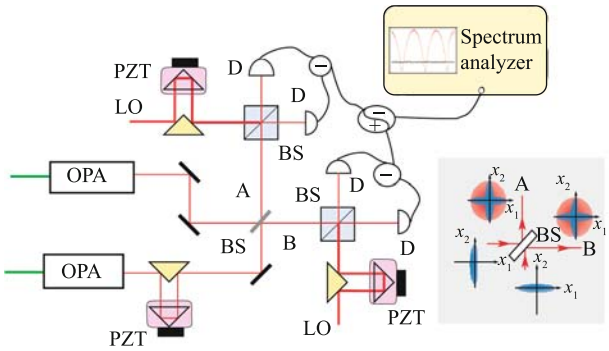

Fig. 19 Experimental setup for generation of entangled state. OPA: optical parametric amplifier, BS: 50:50 beam splitter, L: lens, Ds: photodiodes, PZTs: piezoelectric transducers, and LO: local oscillator.

where $\hat{x}_1^{(0)}$, $\hat{p}_1^{(0)}$, $\hat{x}_2^{(0)}$, and $\hat{p}_2^{(0)}$, are quadrature amplitude and quadrature-phase amplitudes of initial vacua, $\langle\Delta^2\hat{x}_1^{(0)}\rangle = \langle\Delta^2\hat{p}_1^{(0)}\rangle = \langle\Delta^2\hat{x}_2^{(0)}\rangle = \langle\Delta^2\hat{p}_2^{(0)}\rangle = 1$, and r is

a squeezing parameter. By combining these two modes at a half beam splitter, the two output beams become the entangled beams. Output modes ($\hat{a}_A$, $\hat{a}_B$) from the half beam splitter are expressed as

$$\begin{aligned}\hat{a}_A &= \frac{1}{\sqrt{2}}(\hat{a}_1 + \hat{a}_2)\\ \hat{a}_B &= \frac{1}{\sqrt{2}}(\hat{a}_1 - \hat{a}_2)\end{aligned} \tag{7}$$

Thus, amplitude ($\hat{x}_{A/B}$) and phase ($\hat{p}_{A/B}$) quadrature of the output modes ($\hat{a}_A = \hat{x}_A + \mathrm{i}\hat{p}_A$, $\hat{a}_B = \hat{x}_B + \mathrm{i}\hat{p}_B$) show the following correlation:

$$\begin{aligned}\hat{x}_A - \hat{x}_B &= \sqrt{2}\mathrm{e}^{-r}\hat{x}_2^{(0)}\\ \hat{p}_A + \hat{p}_B &= \sqrt{2}\mathrm{e}^{-r}\hat{p}_1^{(0)}\end{aligned} \tag{8}$$

The correlation between pairs of quadratures can be readily written as

$$\begin{aligned}\langle\Delta^2(\hat{x}_A - \hat{x}_B)\rangle &= 2\mathrm{e}^{-2r}\langle\Delta^2\hat{x}_2^{(0)}\rangle\\ \langle\Delta^2(\hat{p}_A + \hat{p}_B)\rangle &= 2\mathrm{e}^{-2r}\langle\Delta^2\hat{p}_1^{(0)}\rangle\end{aligned} \tag{9}$$

i.e., they only depend on the squeezing level. For strong squeezed input states ($r \to \infty$), perfect quantum correlation $\langle\Delta^2(\hat{x}_A - \hat{x}_B)\rangle \to 0$ and $\langle\Delta^2(\hat{p}_A + \hat{p}_B)\rangle \to 0$ are obtained. When we input two coherent states ($r = 0$), we get the shot noise level. The SNL in this case is two units of vacuum noise, because we are considering the cross correlations between two originally independent fields. It is obvious that correlation between modes A and B exist when $r > 0$.

To characterize the entanglement, a well-established approach is to consider the criterion derived by Duan *et al.* [12] and also by Simon [13]. The criterion is based on the total variance of a pair of canonical conjugate variables. It has been demonstrated that, for any separable system, the total variance is bounded from below by a certain value due to the uncertainty relation, whereas for entangled states this bound can be exceeded. The quadratures of electromagnetic fields are a pair of canonical conjugate variables, so the entanglement or equivalently nonseparability can be demonstrated by a violation of the inequality:

$$\langle\Delta^2(\hat{x}_A - \hat{x}_B)\rangle + \langle\Delta^2(\hat{p}_A + \hat{p}_B)\rangle \geqslant 2 \tag{10}$$

Here, the variances of $\langle\Delta^2(\hat{x}_A - \hat{x}_B)\rangle$ and $\langle\Delta^2(\hat{p}_A + \hat{p}_B)\rangle$ are normalized to their SNL.

The scheme, on which the experiment is based, utilizes the superposition of two independently squeezed vacua to create quantum correlations between two output ports in Fig. 19. The detail of generation of squeezed vacuum is described in Section 5. The squeezed vacua produced in the OPAs propagate to a 50:50 beam splitter, where they will spatially overlap and interfere to form the entanglement state. The phase of one of two squeezed vacua is locked so that the squeezing ellipses are perpendicular to each other. Under this condition, the entanglement state was generated which is the quantum resource in quantum information experiments. Each of entanglement beams was measured on a homodyne detector by mixing with an LO light using a beam splitter.

In our experiment, the quality of the entanglement state was investigated both by measuring one entangled beam as well as the correlation between the two entangled beams. The noise in a single entangled beam was measured by fast scanning the local oscillator phase φ of the homodyne detector (200 mHz) while slowly scanning the relative phase θ between the two squeezed vacua (20 mHz). An example is presented in Fig. 20. The observed noise in a single beam of an entangled state was obtained by combining two squeezed vacua with squeezing level of 3.2 dB and 3.0 dB, respectively, while the shot noise level was obtained by blocking the two squeezed vacua inputs. In this run, the rapid sweep of the local oscillator ensures that both quadratures were measured for each value of θ. Hence, the recorded noise of the spectrum analyzer can be expressed by

$$P_N(\varphi) = \cos^2\varphi\langle\Delta^2\hat{x}_A\rangle + \sin^2\varphi\langle\Delta^2\hat{p}_A\rangle \tag{11}$$

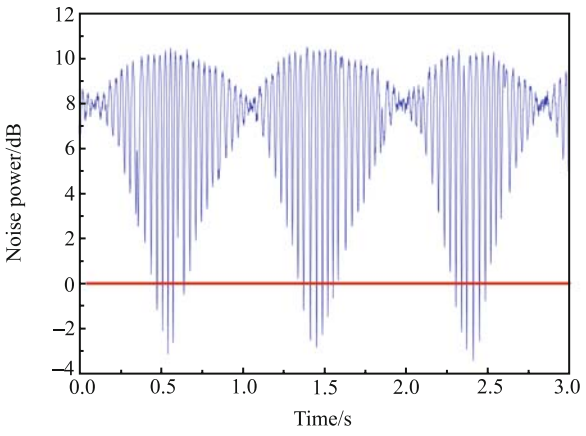

Fig. 20 Normalized noise of one beam of the entangled beams obtained by scanning the mutual phase difference between the two squeezed vacua in addition to a rapid sweep of the LO in the homodyne detector.

Without loss of generality, we assume that both squeezed input vacua have the same variances for the squeezed and the antisqueezed quadrature, $\langle\Delta^2\hat{x}_2\rangle = \langle\Delta^2\hat{p}_1\rangle = V(\delta_{sq})$ and $\langle\Delta^2\hat{x}_1\rangle = \langle\Delta^2\hat{p}_2\rangle = V(\delta_{\mathrm{anti}})$. Depending on the relative interference phase θ, the noise powers of $P_N(\varphi)_{\theta=0} = \cos^2\varphi V(\delta_{sq}) + \sin^2\varphi V(\delta_{\mathrm{anti}})$ at the phase of $\theta = 0$ and $P_N(\varphi)_{\theta=\pi/2} = \frac{1}{2}V(\delta_{\mathrm{anti}})$ at the phase of $\theta = \pi/2$ of a single beam can be directly calculated. As

explained above, the noise of a single beam in Fig. 20 is expected to be phase independent and arises when overlapping two squeezed vacua with a relative phase difference of $\theta = \pi/2$. So, this allows us to identify this point in Fig. 20, and we observed a noise power of about 8 dB, which gives the noise level of the entangled beam, above the shot noise level. Furthermore, the phase sensitive noise is also observed when the two squeezed vacua are combined in phase ($\theta = 0$). The results show a noise reduction of about 3 dB, which equals the noise level of the squeezed vacuum, below shot noise level and the antisqueezing level of more than 10 dB above the shot noise level. As expected, about 3 dB difference between the antisqueezing level and noise level of one entangled beam is observed.

Next, we proceed to the measurement of the entanglement correlation between the two entangled beams via balanced homodyne detection of both and subtracting or adding the resulting photocurrents from the two sets of homodyne systems. In this run, the relative phase (θ) of two squeezed vacua was controlled at $\pi/2$ and one of the LO phases is fixed on measurement one quadrature. The trace in Fig. 21 is a typical recorded noise power spectrum by scanning the LO phase of the second homodyne detection and electronically adding the photocurrents of the two sets of homodyne detectors. The noise power spectrum was normalized to shot noise level, which was obtained by blocking the squeezed vacua inputs. In such a measurement, the noise power of $\hat{x}_A - (\sin\varphi\hat{p}_A + \cos\varphi\hat{x}_B)$ was recorded and the noise reduction of about 2.3 ± 0.2 dB below the shot noise level for two beams was observed when the second homodyne detector measure the same quadrature as the first homodyne detector, i.e., $\varphi = \pi/2$. The correlation of another component between two entangled beams can be measured by fixing the LO phase of the first homodyne detector to ensure measurement of Y quadrature and electronically subtracting, instead of adding, the photocurrents of the two sets of homodyne detectors. In this measurement, the noise power spectrum of $\hat{p}_A + (\sin\varphi\hat{x}_A + \cos\varphi\hat{p}_B)$ is given and the noise reduction of 1.6 ± 0.2 dB below shot noise level was obtained when the second LO phase was chosen as $\varphi = 0$.

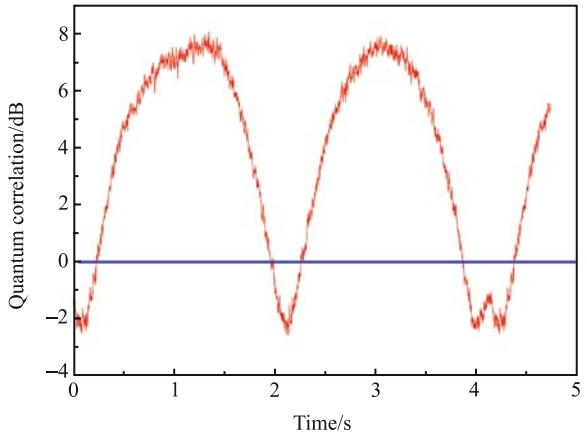

Fig. 21 Entanglement correlation between two entangled beams. It is obtained by adding the signal of two homodyne detectors measuring the two beams while scanning one of the LO phase.

We translate the aforementioned noise reduction into correlation variance and get $\langle\Delta^2(\hat{x}_A - \hat{x}_B)\rangle = 0.59 \pm 0.02$ and $\langle\Delta^2(\hat{p}_A + \hat{p}_B)\rangle = 0.69 \pm 0.02$. The measured values for the correlation variance are plugged into Eq. (10),

$$\langle\Delta^2(\hat{x}_A - \hat{x}_B)\rangle + \langle\Delta^2(\hat{p}_A + \hat{p}_B)\rangle = 1.28 \pm 0.03 < 2 \quad (10)$$

a clear violation of the inequality (10). This result attests for the quantum entanglement of the pulsed state generated by combing two squeezed vacua on a beam splitter. The asymmetry between the correlation measurements between the two components is mainly due to the phase fluctuation on the beam splitter for the entanglement generation, because the component of $(\hat{p}_A + \hat{p}_B)$ is sensitive to the relative phase θ since the drift from $\pi/2$ will introduce the antisqueezing noise to the system.

The other experiment to produce an entangled state by combining two squeezed vacua was performed by Furusawa [89] and his group at the University of Tokyo, Bowen *et al.* [90] and Silberhorn *et al.* [91]. In the first experiment of quantum teleportation, the entangled state was produce by combining two independently squeezed states at a 50:50 beam splitter. The two independently squeezed states were generated from an OPA with folded-ring geometry. Because the OPA is a traveling-wave resonator, it is possible to drive the intracavity nonlinear crystal with two counter propagating pump beams to generate two independently squeezed states counter circulating within the cavity. The OPA was pumped by a frequency doubled single frequency Ti:sapphire laser operating at 866 nm. Both the doubling cavity and the cavity of OPA contain an a-cut $KNbO_3$ crystal for temperature-tuned, noncritical phase matching. Unfortunately, $KNbO_3$ suffers from an inherent loss mechanism that adds to the intracavity losses. This nonlinear loss arises in the OPA in the presence of the blue pump beam and has been termed blue-light-induced infrared absorption (BLIIRA). In the later experiment performed at the University of Tokyo, the degree of entanglement was improved further, by employing PPKTP crystal as nonlinear medium instead of $KNbO_3$ [68]. In the experiment of Bowen *et al.*, each OPA consisted of a semimonolithic MgO:$LiNBO_3$ nonlinear crystal and an output coupler. MgO:$LiNBO_3$ has the advantage over other nonlinear crystals of exhibiting very low levels of

pump induced absorption at the signal and idler wavelengths. The pump field for each OPA was produced by frequency doubling a Nd:YAG laser to 532 nm. Each OPA produced a single squeezed output at 1064 nm, with 4.1 dB of observing squeezing. The squeezed fields were interfered on a 50:50 beam splitter, producing an entangled state of $\langle\Delta^2(\hat{x}_A-\hat{x}_B)\rangle+\langle\Delta^2(\hat{p}_A+\hat{p}_B)\rangle = 0.88\pm0.02$. In the experiment of Silberhorn, the two squeezed beams were generated by exploiting the Kerr nonlinearity of silica fibers along two orthogonal polarization axes of the same polarization maintaining fiber. A degree of $\langle\Delta^2(\hat{x}_A-\hat{x}_B)\rangle+\langle\Delta^2(\hat{p}_A+\hat{p}_B)\rangle = 0.8$ was demonstrated without correcting for detection losses.

6.2 Experiments on generation entanglement state from below threshold nondegenerate OPA/OPO

In the previous section, we described the generation of entanglement by combining two squeezed states from a pair of degenerate OPAs. Another approach is the use of below threshold nondegenerate OPA/OPO. The generation of entanglement state from below threshold NOPA has been extensively investigated in recent years. The principal difficulty of operating the NOPA resides in frequency-degenerate operation. Frequency degeneracy occurs only accidentally since it corresponds to a single point in the experimental parameter space. In experiments with KTP crystals and green pump, the pairing of crystals to compensate walk-off [29] or using a-cut KTP for noncritical phase matching and frequency-doubled Nd:YAP laser [26, 27, 54] was necessary to generate entangled states of light. Recently, Laurat *et al.* proposed a new device — called "self-phase locked NDOPO" — which consists of a type II OPO with a quarter-wave plate inserted inside the cavity [67]. The plate, which can be rotated relative to the principal axis of the crystal, adds a linear coupling between the orthogonally polarized signal and idler fields. It has been demonstrated that the entangled signal and idler fields from the self-phase locked NDOPO show quantum correlations and anticorrelations on orthogonal quadratures for noise frequencies inside the bandwidth of the cavity.

As a matter of fact, the first entanglement correlated fields with continuous variable in an experiment, which was performed by Ou *et al.* in 1992 [26, 27], were generated using an enhanced subthreshold nondegenerate type II intracavity OPO. In their experiment, the enhancement was achieved by placing the non-linear medium inside resonant cavities for each of the pump, signal and idler fields. The pump field at 540 nm was generated by an intracavity frequency doubled Nd:YAP laser, and the non-linear medium was a type II non-critically phase matched KTP crystal. The signal and idler fields produced by a NOPA, were analyzed in a pair of homodyne detectors. By varying the phase of the LO, the detectors could be set to measure either the amplitude or the phase quadrature of the field under interrogation. Strong correlations were observed between the output photocurrents both for joint amplitude quadrature measurement and phase quadrature measurement. To characterize whether their experiment demonstrated the EPR paradox, they used the EPR paradox criterion set out by Reid [5]. They observed a value of $\Delta^2(\hat{x}_s-\hat{x}_i)\Delta^2(\hat{p}_s+\hat{p}_i) = 0.7 < 1$, thereby performing the first direct experimental test of the EPR paradox with continuous variable.

Following the experiment of Ou *et al.*, a coherent injected NOPA was developed at Shanxi University [52]. The merit of injected NOPA is that it can be stably operated at the degeneracy point by locking the cavity on the frequency of the seeder. The frequency degenerate signal and idler outputs of the NOPA can be interfered with each other and produce two coupled modes. It has been demonstrated that such a NOPA is equivalent to two independent degenerate OPAs corresponding to two coupled modes. For the case of balanced input seeders, the superposed coupling modes are squeezed vacuum state and bright squeezed state, respectively [45, 88]. The entangled correlation between the original amplified signal and idler fields can be inferred by measuring the coupled squeezed state. In an experiment, a NOPA with semimonolithic configuration consists of an a-cut type II KTP, the front facet of which was coated to be as the input coupler and the other facet was coated with the dual-band antireflection at pump and sub-harmonic wavelength, as well as a concave mirror of 50-mm-curvature radius, which is used as the output coupler. The pump field at 540 nm and injected sub-harmonic field at 1080 nm are the fundamental and second harmonic field of a home-made Nd:YAP laser. To obtain the frequency-degenerate and balanced signal and idler output, both the b- and c-polarized waves at 1080 nm must resonate simultaneously in a cavity. By fine tuning the crystal temperature, the birefringence between signal and idler waves in KTP is compensated and the simultaneous resonance in the cavity is reached. Instead of direct measurement of the signal and idler, the superposed mode between the signal and idler mode was analyzed. The output of the signal and idler from NOPA was interfered by a 50/50 beam splitter, which consists of a half wave-plate and polarizing beams splitter, to produce two coupled modes. These orthogonally polarized modes, in which one is squeezed vacuum and one is bright squeezed state, have squeezed fluctuation. The squeezed vacuum was measured by the

balance homodyne detector. To eliminate the classical noise, the fundamental light of output from the laser is filtered by a mode cleaner. The transmitted light of the mode cleaner is used as LO to measure the squeezed vacuum. The quadrature-phase amplitude squeezing up to 3.7±0.2 dB is observed. Therefore, the correlation degree of $\langle\Delta^2(\hat{x}_A - \hat{x}_B)\rangle = \langle\Delta^2(\hat{p}_A + \hat{p}_B)\rangle = 0.853 \pm 0.004$ between the quadrature-phase amplitudes of the output entangled beams is directly inferred. The sum of less than 2 showed an entanglement between the amplified signal and idler fields.

In 1998, while working on an optical frequency divider; Mason and Wong [92] and Fabre *et al.* [93] proposed an elegant means of achieving frequency-degenerate operation above threshold. A birefringent plate inside the optical cavity making an angle with the axis of the nonlinear crystal induces a linear coupling between the signal and idler and results in a locking phenomenon that is well known for coupled mechanical or electrical oscillators. This original device is called self-phase locked OPO. Later, it was demonstrated by Laurat *et al.* in 2005 that such a device can also be operated below threshold and exhibits a very rich quantum behavior, such as squeezing and entanglement [67]. The experimental investigation was also carried out by the same group in France. In the experiment of Laurat *et al.*, a triply resonant type II NDOPO, which is pumped by a commercial frequency doubled Nd:YAG laser, was employed. The NDOPO is made of a semimonolithic linear cavity in order to increase the mechanical stability and reduce the reflection losses. A KTP($\theta = 90°$, $\phi = 23.5°$), in which the input flat mirror is directly coated on one facet, is employed as nonlinear media. The output coupler is highly reflecting for the pump and the transmission is 5 % for the infrared. The OPO is actively locked on the pump resonance. The triple resonance is reached by adjustment of both the crystal temperature and the frequency of the pump laser. A $\lambda/4$ plate inserted within the OPO adds a linear coupling between the signal and idler modes which depends on the angle of the plate relative to the principal axes of the crystal. The two superposition modes oriented $\pm 45°$ from the axes of the crystal are linearly coupled between the orthogonally polarized signal and idler fields. The noise of the superposition modes was then characterized for different angles of the plate and quantum correlations and anticorrelations of the signal and idler modes are obtained on nonorthogonal quadratures depending on the angle of the plate. In the case of a very small coupling, an optimal value of the inseparability criterion as low as 0.33±0.02, well below the limit of unity, is measured.

Another experiment to produce the entanglement state was done by Wenger *et al.* [62, 63]. In this experiment, a pulsed entanglement state was generated using a traveling-wave OPA pumped at 423 nm by a frequency doubled pulsed Ti:Sapphire laser beam. A very thin crystal (100 μm) was employed in order to enable broadband phase matching and thus avoiding group-velocity mismatch. The output of the parametric amplifier was then a pulsed two-mode squeezed state with pulse duration of 15 fs and a repetition rate of 780 kHz. In contrast to the mentioned NDOPA, the process used by Wenger *et al.* was driven in a spatially non-degenerate configuration so the signal and idler beams were emitted in two different directions. In this experiment, the entanglement was witnessed by mixing the two EPR beams with relative phase shift at a 50:50 beam splitter and then monitoring one output using a homodyne detector. The measured nonseparability of 1.4 was obtained.

6.3 Experiments on generation entanglement from above threshold NDOPO

The existence of entanglement between amplitude and phase quadratures of intense signal and idler modes produced from an NDOPO operating above threshold was theoretically predicted by Reid and Drummond in 1988 [5] and then was successively analyzed with detailed theoretical calculations [11, 94]. However, phase correlation of the twin beams was not observed for a long time owing to technical difficulty in measuring the phase noise of twin beams. The basic difficulty in measuring phase fluctuations, in contrast with intensity fluctuations, is that the standard technique, homodyne detection, calls for a LO having a well-defined phase relationship with the field to be measured. In the NDOPO, this is difficult to implement, since the frequencies of the twin beams are usually different, depending on the oscillating modes, and vary from one realization to the next. Hence, two LOs would be required: one for each beam. Furthermore, it would also be necessary to phase lock these fields to the twin beams. In practice, it is impossible to obtain such LOs. Therefore, the measurement of multicolored entangled beams is challenging in experiments.

To break this obstacle, one approach is to force the NDOPO to oscillate in a strict frequency degenerate situation. This is technically challenging and has been done by two groups using different techniques [7, 23]. Laurat *et al.* [23] forced the NDOPO to oscillate in a strict frequency-degenerate situation by inserting a $\lambda/4$ wave plate inside the NDOPO, called self-phase-locked OPO, and observed a 4.5 dB intensity variance below the SNL but 3 dB phase-sum variance above the SNL when the OPO is operating above its threshold. In con-

trast to the technique of self-phase locked OPO, another technique, called phase-difference-lock OPO [7], is to actively lock the frequency difference between the signal and idler to zero. In this experiment, a new nonlinear material Na:KTP, in which the noncritical and collinear phase matching from 532 nm to 1064 nm can be achieved at room temperature, is employed. Such a system allows the convenient use of highly stable Nd:YAG lasers. With only the temperature and cavity locks, the frequency difference error between the signal and idler outputs from OPO is ±150 kHz when the OPO is operating above its threshold. To further reduce the fluctuations, a phase-lock loop is added to the OPO system. In this phase lock loop, the optical frequency difference between signal and idler beams from OPO is detected by beating each other and the result beat signal is phase locked to a stable synthesized radio frequency, by applying a correction voltage along the z-axis of the crystal to change the refraction indexes of the crystal via the electro-optic modulation effect. Adding this phase lock loop reduces frequency difference error by more than 5 orders of magnitude to less than 1 Hz. Hence, the frequency degenerate operation of OPO is obtained. In principle, both the intensity-difference and phase-sum fluctuation can be detected by combining the signal with a LO. As an experiment result, the intensity-difference squeezing of -3 dB is observed by direct detecting the signal and idler beams when LO beams are blocked. To observe the phase-sum noise, two simultaneous frequency upshift and downshift LOs are combined with the signal and idler, respectively. The quadrature-sum noise was measured when one of the LO phases was locked at the measurement of phase-quadrature versus the other LO phase and a phase-sum squeezing of -1.35 dB was obtained. Together with the intensity difference squeezing, a Duan-Simon criterion of $\langle\Delta^2(\hat{x}_A - \hat{x}_B)\rangle + \langle\Delta^2(\hat{p}_A + \hat{p}_B)\rangle = 1.24 < 2$ was obtained. This demonstrated the realization of entanglement between the signal and idler beams when the OPO is operating above its threshold.

An alternative approach is to perform self-homodyne measurement, without the use of LO. The advantage of this approach is that it can measure the multicolored entangled beams. The bipartite two-color entanglement, which has been done very recently, was observed in the above-threshold OPO by two groups. In one group, the self-homodyne was carried out by a pair of tunable ring analysis cavity [8]. Villar *et al.* performed the experiment with a triply resonant OPO pumping by a commercial Nd:YAG laser at a wavelength of 532 nm and operating above its threshold. The orthogonally polarized twin beams are produced and separated by a PBS cube and each directed to a tunable ring analysis cavity. The reflected field is detected by a high quantum efficiency photodiode and analysis. It has been extensively demonstrated that the analysis cavity can completely convert incident phase fluctuations into amplitude fluctuations of the reflected beam dependence on the cavity detuning (Δ). In particular, when $\Delta = 0$, the amplitude noise of the reflected beam comes from the amplitude noise of the incident fields; however, the phase fluctuation of the incident beam are projected into amplitude fluctuations of the reflected beam for $\Delta = \pm\delta\nu_{\rm ac}/2$, where $\delta\nu_{\rm ac}$ is the cavity bandwidth of the analysis cavity. Using the analysis cavity, the sum and difference of quadrature fluctuations between that of the signal and idler beams from above threshold OPO is analyzed. Phase anticorrelation of 0.8 dB below the SNL for a pump power of 4 % above threshold was measured. Together with amplitude correlation of 0.59, $\langle\Delta^2(\hat{x}_A - \hat{x}_B)\rangle + \langle\Delta^2(\hat{p}_A + \hat{p}_B)\rangle = 1.41 < 2$ was obtained, a clear violation of the Duan-Simon criterion, characterizing entanglement between two bright beams. At almost the same time, Su *et al.* [9] were also devoting their effort to measuring the phase anticorrealtion using another approach. In their experiment, a Nd:YAP/KTP above threshold OPO system is established and two sets of unbalanced Mach-Zehnder (M-Z) interferometers are employed to measure the phase correlation. For an unbalanced M-Z interferometer, when the relative phase shift between two optical fields that pass through the short arm and through the long arm is adjusted to $\pi/2 + 2k\pi$(where k is an integer), and the phase shift of the spectral components is controlled to π [95], the fluctuations of the sum and the difference photocurrents of two output fields from the M-Z interferometer in frequency domain is proportional to the SNL and the spectral component of the phase quadrature of the initial field. In the experiment of Su *et al.*, the results show that the correlation variance of the intensity difference and phase sum between the twin beams are below the SNLs of twin beams of 2.58 and 1.05 after accounting for the influences of the electronic noise of the detector. The sum of the correlation variance of the amplitude and phase quadratures of the twin beams is $\langle\Delta^2(\hat{x}_A - \hat{x}_B)\rangle + \langle\Delta^2(\hat{p}_A + \hat{p}_B)\rangle = 1.332 < 2$. Thus, the quantum entanglement between the signal and idler beams is experimentally proved. These experiments open a newway for the measurement of multicolored quantum entanglement and quantum information experiments. The quantum correlation existing among the three output fields (pump, signal, and idler) of a triply resonant OPO operating above threshold are theoretically calculated and experimentally demonstrated [96, 97].

7 Applications of non-classical state

In the early years after the squeezed state experiment, the application of the squeezed state has been experimentally demonstrated to improve the sensitivity of precision optical measurements beyond the SNL. For example, squeezed vacuum states have been used to improve the precision of SNL measurement of weak absorption and in an interferometer [98, 99]. Later, continuous quantum nondemolition (QND) measurements of the amplitude quadrature were performed with a monolithic dual-port degenerate optical parametric amplifier (OPA) and beam splitter [100, 101]. After it was successfully applied in quantum teleportation of coherent states in 1998 [89], the application of squeezed state has been focused on the new branch of physics–quantum information with continuous variables. Important continuous variable experiments include the dense-coding experiment of Li *et al.* [102], the demonstration of a quantum memory effect [103, 104] and quantum network [105]. The details of quantum information with continuous variables can be found in the review papers of Braunstein and van Loock [1] and Furusawa [106]. In this section, we focus on the application of the twin beams.

Similar to the squeezed state, the twin beams can be applied to measurements beyond the SNL [107] and QND measurement [108], communications, spectroscopy [109] and a range of other fields. Here, we give an example of the application of twin beams in quantum communications channel. Furthermore, an experiment of sub-shot-noise-recovery in the measurement using twin beams is also presented.

7.1 Sub-shot-noise-recovery measurement

An experimental setup for sub-shot-noise-recovery measurement is shown in Fig. 22. After the twin beams are separated into the signal and idler beams with the PBS, the idler beam is detected by a photodiode. The amplitude of the signal beam is modulated near 4 MHz in an electro-optical modulator (EOM), and then detected by a photodiode. An intensity attenuator (ATT) is inserted in the arm of the idler beam to balance the dc photocurrents in the signal and the idler channels. The outputs of two photodiodes are amplified and subtracted at a 180° power combiner (−). The noise of the differential photocurrent is recorded by a spectrum analyzer in the frequency domain or by an oscilloscope in the time domain using the down-conversion technique described in Section 6. In Fig. 23, curve (a) is the result measured with coherent light, the intensity of which is exactly equal to that of the twin beams used in the measurement. Curve (b) is obtained with the twin beams of quantum correlation. It is obvious that because of the reduction of noise the signal-to-noise ratio is improved approximately 4.2 dB in curve (b).

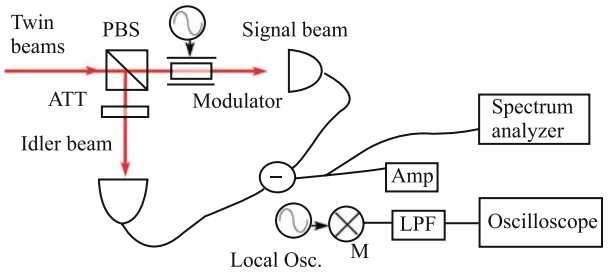

Fig. 22 Experimental setup for sub-shot-noise-recovery measurment. ATT: attenuator, Amp: amplifier, LPF: low pass filter, M: mixer; PBS: polarizing beam splitter.

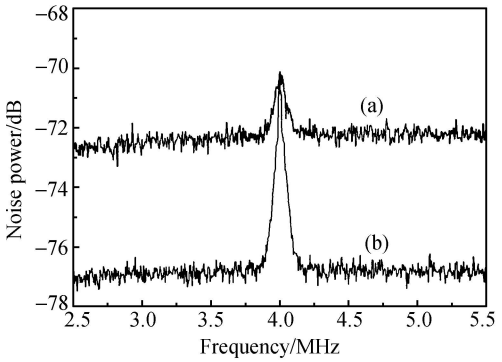

Fig. 23 Recovery of quantum signal in frequency domain. Trace **(a)** is the measured signal using coherent light. Trace **(b)** is measured signal using twin beams.

The weak sub-shot-noise-recovery measurement in the time domain is presented in Fig. 24, in this run, the modulation signal is adjusted to bury in the shot noise when coherent light is employed as light source. Figure 24 (a) shows the condition in which the weak modulation signal is buried in the shot noise. It was obtained by mixing the amplified photocurrents with a local oscillator for down conversion to 50 kHz, and the down-converted

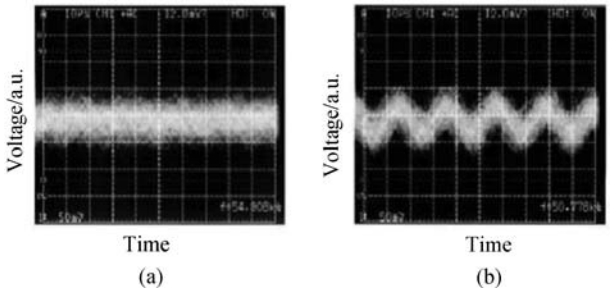

Fig. 24 Recovery of quantum signal in time domain. **(a)** The transmitted signal is hidden by the shot noise. **(b)** The transmitted signal is recovered using twin beams.

weak signal, after passing through a low-pass filter, was recorded with an oscilloscope. In Fig. 24 (b), the shot noise is canceled using the quantum correlated twin beam, and a weak signal—modulated below the SNL—can be recognized.

7.2 Quantum channel with twin beams

The proposal given by Funk and Raymer [110] uses two different polarization bases, which are used in our experiment. One basis (V/H basis) is defined by the vertical and horizontal linear polarizations; the other basis (± 45 basis) is defined by the $\pm 45°$ linear polarization and $-45°$ linear polarization. Alice encodes each bit value in the mean photon difference number $\langle n\rangle = \langle n_1\rangle - \langle n_2\rangle$, where $\langle n_1\rangle$ ($\langle n_2\rangle$) is the mean number of photons in the first (second) polarization mode making up a basis. Alice encodes a logical key in either V/H basis or ± 45 basis. Bob measures the photon number difference either in the V/H or in the ± 45 basis. Thus, photon number difference in the correct bases, which means Alice and Bob use the same basis, is $n_{\rm V} - n_{\rm H}$ in V/H basis and $n_{+45°} - n_{-45°}$ in the ± 45 basis, respectively. Alice encodes a logical "1" ("0") key bit by setting the mean value of the difference number to be in the correct basis $\langle n\rangle = N$ ($\langle n\rangle = -N$), where N is a positive number. The photon number difference N is small ($\leqslant 1\,\%$) compared with $\langle n_{\rm V}\rangle$ and $\langle n_{\rm H}\rangle$, which should contain more than 10^4 photons on average. After all the key bits have been transmitted, Alice and Bob communicate via a public channel and compare the bases they used for each encoding/measurement. Alice and Bob can separate their communications wrong basis and uncorrected basis dependence using the same and difference basis.

For the correct-basis measurement, Bob sets the threshold N_0 and constructs his bit sequence by using the following decision:

$$\text{bit value} = \begin{cases} 1, & \text{if} \quad \langle n\rangle > N_0 \\ 0, & \text{if} \quad \langle n\rangle < N_0 \\ \text{inconclusive otherwise} \end{cases} \tag{13}$$

where $\langle n\rangle$ is the result of Bob's photon number difference measurement. Alice's bit values are determined by the photon number difference: She regards $\langle n\rangle = N$ as "1" and $\langle n\rangle = -N$ as "0". Due to the tails of the distribution for the two bit values, there is a nonzero probability that a key bit encoded by Alice as a logical "1" ("0") would be measured by Bob as "0" ("1"). Such an error is a bit error. Because the photon difference variance of the twin beams is less than that of coherent state, the bit error rate can be reduced by using the twin beams as a signal carrier.

Figure 25 shows the experimental setup of our quantum channel. At Alice's station, an NDOPO pumped above its threshold by a diode-pumped continuous wave (CW) frequency-doubled YAG laser emits quantum correlated twin beams. A detailed description of the NDOPO can be found in Section 6. In this experiment, the intensity correlation between the twin beams is reduced to about -5.5 ± 0.3 dB. The orthogonal polarized twin beams, which correspond to V- and H-polarized modes, are separated by a $\rm PBS_1$. An attenuator (1 %), which weakly affects the quantum correlation between the two modes of the twin beams, is inserted in the vertical or horizontal light's path. The attenuator generates the mean value of the difference in photon number between the two modes (either N or $-N$) so that the logical key bit is encoded. The two beams are then combined by another polarizing beam splitter (PBS2). A half-wave plate, which is rotated by an angle of $0°$ or $\pm 45°$, is inserted into the beam paths before the twin beams are sent to Bob. As the experimental measurement, when the two beams are rotated by an angle of $0°$ with respect to its axes, the V/H basis is selected, and when the polarizations of the two beams is rotated by an angle of $45°$, the ± 45 basis is selected. At Bob's station, he measures the photon number difference $\langle n\rangle$ in either the V/H basis or the ± 45 basis, which is chosen at random using the half-wave plate, PBS3, and a pair of balanced high quantum efficiency photodiodes. By biasing the two diodes with opposite polarity and summing their output,

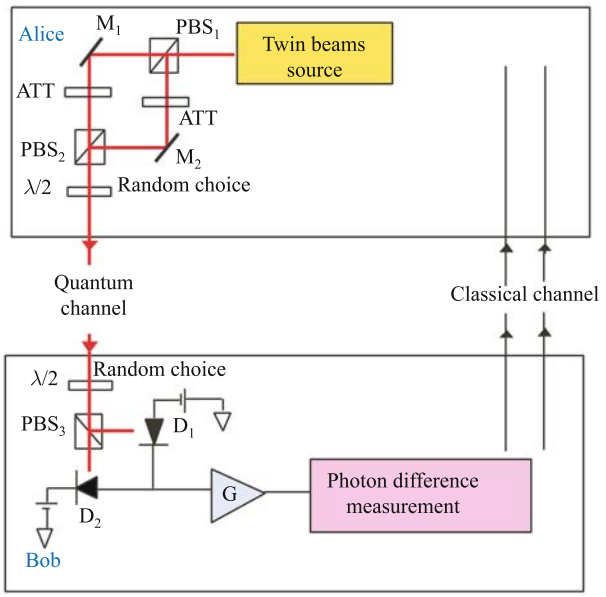

Fig. 25 Schematic of the experimental setup. PBS: polarizing beam splitter; $\rm D_1$ and $\rm D_2$: detector; G: low noise electronic amplifier; $\rm M_1$ and $\rm M_2$: mirror.

one obtains the difference in current. The current is detected with a low-noise amplifier (CLC425), which we accurately calibrated. In order to correctly detect the logical key bit, the beams are rotated by an angle of 0° or −45° at Bob's station. In this situation, the vertical and the horizontal polarization mode from the NDOPO always beat detector D_1 and D_2 in the correct basis, respectively. For comparison with a system implementing with a classical coherent state, the coherent light is input onto another port of PBS_1 (not shown in Fig. 1). In the experiment, we could block either the coherent light or twin beams to measure the probability distribution in photon number difference of the system. The BER of our system is measured when either the coherent light is blocked or the twin beams.

We have implemented the same technique as in Section 6 by measuring the photon number difference between two beams at a given Fourier frequency Ω. The difference in photocurrents is amplified and multiplied by a sinusoidal current of frequency Ω produced by a signal generator, and filtered by a 100 kHz low-pass filter in order to obtain the instantaneous value of the photocurrent Fourier component at frequency Ω, which is then recorded by an A/D board installed in a PC, which also simultaneously records the instantaneous value of the DC photocurrent. Figure 26 shows the photo-electron difference probability distribution of the system implemented with coherent light and twin beams in correct basis and incorrect basis. It was obtained by subdividing about 100 000 experimental data, which were obtained with a demodulation frequency Ω =4 MHz, into 100 equal-interval bins. The width of bin, δN, is about 20. The average photoelectron number of each detector was scaled to be $\langle n_1\rangle = \langle n_2\rangle = 4\times10^4$, and the photoelectron difference was fixed at N =200, which is about 0.5 % of the total photon number. The measured mean and standard deviation are listed in Table 3. Theoretical probability distributions from the equation with N =200 and standard derivation $\delta_{\rm twin}$ =145±10 for twin beams, which corresponds to a 70 % reduction in the noise below the SNL, and $\delta_{\rm coh}$ =270±10 for coherent beams are also shown in Fig. 26. To fit the theoretical prediction, a fixed coefficient was introduced to scale all probabilities of the experiment. The bit error rate of our system will be 0.067 using the twin beams compared with 0.217 using the coherent state as the signal carrier. We should mention that our quantum communication channel could be used for quantum key distribution as the Funk and Raymer's protocol. The security of the key is ensured by using the quantum correlation between the signal and idler of the two beams. The quantum correlation between the orthogonal polarization modes is rapidly degraded by any attempt by an eavesdropper (Eve) to measure the key. Degradation in the correlation would lead to an increase in the BER that would indicate to Bob and Alice the presence of Eve.

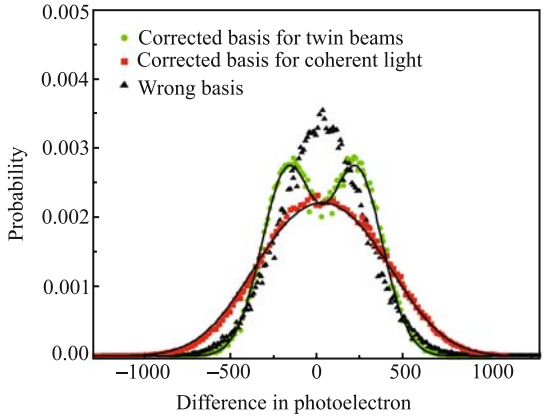

Fig. 26 Measured distributions of photoelectrons difference of twin beams and coherent light in correct and incorrect basis. Solid line: theoretical prediction; Symbols: experimental result; Circles: for twin beams in correct basis; Squares: for coherent light in correct basis; Triangles: in wrong basis.

Table 3 Measured mean and standard derivation of different bases when the system is implemented with coherent state and twin beams.

	Pre selection		Photon number difference	
Sources	Basis selection	Key	Mean	Standard deviation
Twin beams	Corrected basis	1	200	145±10
	Corrected basis	0	−200	145±10
	Wrong basis	1	0	270±10
	Wrong basis	0	0	270±10
Coherent light	Corrected basis	0	200	270±10
	Corrected basis	1	−200	270±10
	Wrong basis	0	0	270±10
	Wrong basis	1	0	270±10

8 Outlook and conclusion

Since the first realization of the squeezed state from OPO/A, its generation has been improved through a series of important developments, both theoretical and technological. To date, it is not so difficult to produce a squeezed state with more than 5 dB noise reduction and several hours stability from an enhanced cavity. The noise reduction of pulsed squeezed state is also improved by employing waveguides, in which the spatial profile of light is determined. In other words, the improvements of generation of squeezed state make the creation of stable entangled state possible. For the further development of the generation and implementation of squeezed state, we believe that it will be to develop a more com-

pact and reliable squeezed state source. Although it is not so difficult to produce a large amount of squeezed state, it is not easy to keep the squeezing degree since the squeezed state is fragile and sensitive to the phase fluctuations. Furthermore, the generation system is very luxurious and the operating system requires a specialist. In order to extend the application of squeezed state, it is time to reduce the cost and simplify the operation of the generation system.

At present, the application of the squeezed state is focused on the quantum information with continuous variables. The most prominent examples of quantum information are quantum teleportation, quantum computation and quantum key distribution. In principle, quantum teleportation is the reliable transfer of quantum information through a classical channel using shared entanglement. Quantum computation means in particular cases, in principle, as computation that is faster than any known classical computation, while quantum key distribution makes possible unconditionally secure communication as opposed to classical key distribution. Although the principled experiments in quantum information, such as quantum teleportation, have been carried out, in order to come closer to real applications, both for long-distance quantum communication and for quantum computation, a new generation of experiments and technologies are needed. The fragile squeezed state can only be implemented in a laboratory without being significantly influenced by a noisy environment.

In my opinion, the potential application of squeezed state may lie on the test of the fundamental principle of physics, such as the demonstration of EPR paradox. Up to know, the demonstration of EPR paradox has been realized through lots of experiments, which can be classified into manipulation of discrete systems, such as spin and polarization of photon, or manipulation of continuous variables, such as the quadrature amplitudes of electromagnetic fields. With the continuous variable, implementations always work efficiently and unconditionally, but never perfectly and causally; counterparts only work sometimes (conditioned upon rare successful events) but they succeed, in principle, perfectly and causally with discrete variable. The overlap between the continuous and discrete regime may overcome this barrier. Condition state preparation was originally used to prepare a single photon state from quantum correlated photons generated via SPDC [111]. Now, it is used to link the discrete regime with the continuous regime, i.e., continuous detecting on continuous variables conditioned by a photon counting event. So far, some remarkable experiments have been carried out using this technique, such as generation of a "degaussification" state [112], generation of new quantum states [113, 114], entanglement purification [115], and generation of a Schrödinger-cat state [116−118]. Further improvement with more specialized technology makes the casual and efficient demonstration of EPR paradox not impossible. By using field quadrature measurement and multi-particle states, quantum theory and its alternatives may also be tested for increasingly macroscopic systems.

Acknowledgements The work of generation of squeezed and entangled state from a single-pass OPAs was carried out with Profs. T. Hirano and Mr. R. Okubo at Gakushuin University. The other experimental results described in this paper were accomplished by collaboration with Dr. Kasai, Mr. Hayasaka and Prof. Watanabe (presently at the University of Electro-Communications) at the National Institute of Information and Communications Technology.

References

1. S. L. Braunstein and P. van Loock, Rev. Mod. Phys., 2005, 27: 513
2. S. Braunstein and A. K. Pati, Quatum Information with Continuous Variables, Dordrecht: Kluwer Akademic Press, 2003
3. A. Aspect, J. Dalibard, and G. Roger, Phys. Rev. Lett., 1982, 49: 1804
4. D. Bouwmeester, A. K. Ekert, and A. Zeilinger, The Physics of Quantum Information, Springer, 2000
5. M. D. Reid and P. D. Drummond, Phys. Rev. Lett., 1988, 60: 2731
6. M. D. Reid and P. D. Drummond, Phys. Rev. A, 1989, 40: 4493
7. J. T. Jing, S. Feng, R. Bloomer, and O. Pfister, Phys. Rev. A, 2006, 74: 041804(R)
8. A. S. Villar, L. S. Cruz, K. N. Cassemiro, M. Martinelli, and P. Nussenzveig, Phys. Rev. Lett., 2006, 95: 243603
9. X. L. Su, A. H. Tan, X. J. Jia, Q. Pan, C. D. Xie, and K. C. Peng, Opt. Lett., 2006, 31: 1133
10. R. J. Glauber, Phys. Rev., 1963, 131: 2766
11. C. Fabre, E. Giacobino, A. Heidmann, and S. Reynaud, J. Phys. France, 1989, 50: 1209
12. L. M. Duan, G. Giedke, J. I. Cirac, and P. Zoller, Phys. Rev. Lett., 2000, 84: 2722
13. R. Simon, Phys. Rev. Lett., 2000, 84: 2726
14. R. E. Slusher, L. W. Hollberg, B. Yurke, J. C. Mertz, and J. F. Valley, Phys. Rev. Lett., 1985, 55: 2409
15. L. A. Wu, H. J. Kimble, J. H. Hall, and H. Wu, Phys. Rev. Lett., 1986, 57: 2520
16. L. A. Wu, M. Xiao, and H. J. Kimble, J. Opt. Soc. Am. B, 1987, 4: 1465
17. K. Schneider, R. Bruckmeier, H. Hansen, S. Schiller, and J. Mlynek, Opt. Lett., 1996, 21: 1396
18. K. Schneider, M. Lang, J. Mlynek, and S. Schiller, Opt. Express, 1998, 2: 59
19. Y. Takeno, M. Yukawa, H. Yonezawa, and A. Furusawa,

Opt. Express, 2007, 15: 4321
20. H. Vahlbruch, M. Mehmet, N. Lastzka, B. Hage, S. Chelkowski, A. Franzen, S. Gossler, K. Danzmann, and R. Schnabel, Phys. Rev. Lett., 2008, 100: 033602
21. J. Mertz, T. Debuisschert, A. Heidmann, C. Fabre, and E. Giacobino, Opt. Lett., 1991, 16: 1234
22. J. R. Gao, F. Y. Cui, C. Y. Xue, C. D. Xie, and K. C. Peng, Opt. Lett., 1998, 23: 870
23. J. Laurat, L. Longchambon, C. Fabre, and T. Coundreau, Opt. Lett., 2005, 30: 1177
24. K. McKenzie, N. Grosse, W. P. Bowen, S. E. Whitcomb, M. B. Gray, D. E. McClelland, and P. K. Lam, Phys. Rev. Lett., 2004, 93: 161105
25. Y. Zhang, K. Hayasaka, and K. Kasai, Opt. Express, 2006, 14: 13083
26. Z. Y. Ou, S. F. Pereira, H. J. Kimble, and K. C. Peng, Phys. Rev. Lett., 1992, 68: 3663
27. Z. Y. Ou, S. F. Pereira, and H. J. Kimble, Appl. Phys. B, 1992, 55: 265
28. M. E. Anderson, D. F. McAliser, M. G. Raymer, and M. C. Gupta, J. Opt. Soc. Am. B, 1997, 14: 3180
29. P. Gragier, R. E. Slusher, B. Yurke, and A. LaPorta, Phys. Rev. Lett., 1987, 59: 2153
30. R. E. Slusher, P. Gragier, A. LaPorta, B. Yurke, and M. J. Potasek, Phys. Rev. Lett., 1987, 59: 2566
31. A. Heidmann, R. Horowica, S. Reynaud, E. Giacobino, C. Fabre, and G. Camy, Phys. Rev. Lett., 1987, 59: 2555
32. C. D. Nabors and R. M. Shelby, Phys. Rev. A, 1990, 42: 556
33. P. Kumar, O. Aytur, and J. Huang, Phys. Rev. Lett., 1990, 64: 1015
34. T. Hirano and M. Matsuoka, Opt. Lett., 1990, 15: 1153
35. O. Aytur and P. Kumar, Phys. Rev. Lett., 1990, 65: 1551
36. R. Movshovich, B. Yurke, P. G. Kaminsky, A. D. Smith, A. H. Silver, R. W. Simon, and M. V. Schneider, Phys. Rev. Lett., 1990, 65: 1419
37. S. F. Pereira, K. C. Peng, and H. J. Kimble, in: Coherence and Quantum Optics VI, edited by J. H. Eberly, L. Mandel, and E. Wolf, New York: Plenum, 1990: 497
38. O. Aytur and P. Kumar, Opt. Lett., 1992, 17: 529
39. R. M. Shelby and M. Rosenbluh, Appl. Phys. B, 1992, 55: 226
40. P. Kurz, R. Paschotta, K. Fiedler, A. Sizmann, G. Leuchs, and J. Mlynek, Appl. Phys. B, 1992, 55: 216
41. T. Hirano and M. Matsuoka, Appl. Phys. B, 1992, 55: 233
42. E. S. Polzik, J. Carri, and H. J. Kimble, Appl. Phys. B, 1992, 55: 279
43. D. T. Smithey, M. Beck, M. G. Raymer, and A. Faridani, Phys. Rev. Lett., 1993, 70: 1244
44. K. C. Peng, M. Q. Huang, J. Liu, Y. M. Lian, T. C. Zhang, C. Yu, C. D. Xie, and G. C. Guo, Acta Physica Sinica, 1993, 42: 1079 (in Chinese)
45. C. Kim and P. Kumar, Phys. Rev. Lett., 1994, 73: 1605; C. Kim, R. D. Li, and P. Kumar, Opt. Lett., 1994, 19: 132
46. M. E. Anderson, M. Beck, M. G. Raymer, and J. D. Bierlein, Opt. Lett., 1995, 20: 620
47. D. K. Serkland, M. M. Fejer, R. L. Byer, and Y. Yamamoto, Opt. Lett., 1995, 20: 1649
48. G. Breitenbach, T. Muller, S. F. Pereira, J. P. Poizat, S. Schiller, and J. Mlynek, J. Opt. Soc. Am. B, 1995, 12: 2304
49. Q. Pan, Y. Zhang, T. C. Zhang, C. D. Xie, and K. C. Peng, J. Phys. D: Appl. Phys., 1997, 30: 1588
50. K. C. Peng, Q. Pan, H. Wang, Y. Zhang, H. Su, and C. D. Xie, Appl. Phys. B, 1998, 66: 755
51. J. Teja and N. Wong, Opt. Express, 1998, 2: 65
52. P. K. Lam, T. C. Ralph, B. C. Buchler, D. E. McClelland, H.-A. Bachor, and J. R. Gao, J. Opt. B, 1999, 1: 469
53. M. Vasilyev, S. K. Choi, P. Kumar, and D'Ariano G. Mauro, Phys. Rev. Lett., 2000, 84: 2354
54. Y. Zhang, H. Wang, X. Y. Li, J. T. Jing, C. D. Xie, and K. C. Peng, Phys. Rev. A, 2000 62: 023813
55. R. X. Guo, J. Laurat, J. R. Gao, C. D. Xie, and K. C. Peng, Appl. Opt., 2002, 41: 2304
56. R. X. Guo, X. J. Jia, C. D. Xie, and K. C. Peng, Opt. Commun., 2002, 211: 243
57. Y. Zhang, K. Kasai, and M. Watanabe, Opt. Lett., 2002, 27: 1244
58. S. Feng and O. Pfister, J. Opt. B: Quantum Semiclass. Opt., 2003, 5: 262
59. U. L. Andersen, B. C. Buchler, P. K. Lam, J. W. Wu, J. R. Gao, and H.-A. Bachor, Eur. Phys. J. D, 2003, 27: 181
60. H. B. Wang, Z. H. Zhai, S. K. Wang, and J. R. Gao, Europhys. Lett., 2003, 64: 15
61. J. Laurat, T. Coudreau, G. Keller, N. Treps, and C. Fabre, Phys. Rev. A, 2004, 70: 042315
62. K. Hayasaka, Y. Zhang, and K. Kasai, Opt. Lett., 2004, 29: 1665
63. J. Wenger, R. Tualle-Brouri, and P. Grangier, Opt. Lett. 2004, 29: 1267
64. J. Wenger, A. Ourjoumtsev, R. Tualle-Brouri, and P. Grangier, Eur. Phys. J. D, 2005, 32: 391
65. T. Hirano, K. Kotani, T. Ishibashi, S. Okude, and T. Kuwamoto, Opt. Lett., 2005, 30: 1722
66. J. Mizuno, K. Wakui, A. Furusawa, and M. Sasaki, Phys. Rev.A, 2005, 71: 012304
67. J. Laurat, T. Coudreau, G. Keller, N. Treps, and C. Fabre, Phys. Rev. A, 2005, 71: 022313
68. S. Suzuki, H. Yonezawa, F. Kannari, M. Sasaki, and A. Furusawa, Appl. Phys. Lett., 2006, 89: 061116
69. Y. Eto, T. Tajima, Y. Zhang, and T. Hirano, Jpn. J. Appl. Phys., 2006, 45: L821
70. T. Aoki, G. Takahashi, and A. Furusawa, Opt. Express, 2006, 14: 6930
71. T. Tanimura, D. Akamatsu, Y. Yokoi, A. Furusawa, and M. Kozuma, Opt. Lett., 2006, 31: 2344
72. H. Vahlbruch, S. Chelkowski, B. Hage, A. Franzen, K. Danzmann, and R. Schnabel, Phys. Rev. Lett., 2006, 97: 011101
73. G. Hetet, O. Glockl, K. A. Pilypas, C. C. Harb, B. C. Buchler, H.-A. Bachor, and P. K. Lam, J. Phys. B: At. Mol. Opt.

Phys., 2007, 40: 221
74. K. Yoshino, T. Aoki, and A. Furusawa, Appl. Phys. Lett., 2007, 90: 041111
75. Y. Eto, T. Tajima, Y. Zhang, and T. Hirano, Opt. Lett., 2007, 32: 1698
76. M. Bondani, A. Allevi, G. Zambra, M. G. A. Paris, and A. Andreoni, Phys. Rev. A, 2007, 76: 013833
77. Y. Zhang, T. Furuta, R. Okubo, K Takhashi., and T. Hirano, Phys. Rev. A, 2007, 76: 013833
78. M. Lassen, M. Sabuncu, P. Buchhave, and U. Andersen, Opt. Express, 2007, 15: 5077
79. K. Goda, E. E. Mikhailov, O. Miyakawa, S. Saraf, S. Vass, A. Weinstein, and N. Mavalvala, 2007, arXiv: 0703001
80. D. H. Lee, M. E. Klein, and K. J. Boller, Appl. Phys. B, 1998, 66: 747
81. A. Porzio, C. Altucci, P. Aniello, C. de Lisio, and S. Solimeto, Appl. Phys. B, 2002, 75: 655
82. A. Porzio, F. Sciarrino, A. Chiummo, M. Fiorentino, and S. Solimeno, Opt. Commun., 2001, 194: 373
83. Y. Zhang, K. Kasai, K. Hayasaka, J. Opt. Soc. Am. B, 2004, 21: 1044
84. A. Porzio, C. Altucci, P. Aniello, A. Chiummo, C. de Lisio, and S. Solimeto, J. Opt. Quantum Semiclassical Opt. 2002, 4: S313
85. Y. Zhang, K. Kasai, and M. Watanabe, Phys. Lett. A, 2002, 297: 29
86. G. Breitenbach and S. Schiller, J. Mod. Opt., 1997, 44: 2207
87. Y. Zhang, K. Hayasaka, and K. Kasai, Appl. Phys. B, 2007, 86: 643
88. Y. Zhang, H. Su, C. D. Xie, and K. C. Peng, Phys. Lett. A, 1999, 259: 171
89. A. Furusawa, J. Sørensen, S. L. Braunstein, C. A. Fuchs, H. J. Kimble, and E. Polzik, Science, 1998, 282: 706
90. W. P. Bowen, R. Schnabel, P. K. Lam, T. C. Ralph, Phys. Rev. Lett., 2004, 90: 043601
91. Ch. Silberhorn, P. K. Lam, O. Weiß, F. König, N. Korolkova, and G. Leuchs, Phys. Rev. Lett., 2001, 86: 4267
92. E. J. Mason and N. C. Wong, Opt. Lett., 1998, 23: 1733
93. C. Fabre, E. J. Mason, and N. C. Wong, Opt. Commun., 1999, 170: 299
94. A. S. Villar, M. Martinelli, and P. Nussenzveig, Opt. Commun., 2004, 241: 551
95. O. Glockl, U. L. Andersen, S. Lorenz, Ch. Silberhorn, N. Korolkova, and G. Leuchs, Opt. Lett., 2004, 29: 1936
96. A. S. Villar, M. Martinelli, C. Fabre, and P. Nussenzveig, Phys. Rev. Lett., 2006, 97: 140504
97. K. N. Cassemiro, A. S. Villar, P. Valente, M. Martinelli, and P. Nussenzveig, Opt. Lett., 2006, 32: 695
98. M. Xiao, L. A. Wu, and H. J. Kimble, Phys. Rev. Lett., 1987, 59: 278
99. P. Grangier, R. E. Slusher, B. Yurke, and A. LaPorta, Phys. Rev. Lett., 1987, 59: 2153
100. R. Bruckmeier, K. Schneider, S. Schiller, and J. Mlynek, Phys. Rev. Lett., 1997, 78: 1243
101. R. Bruckmeier, H. Hansen, S. Schiller, and J. Mlynek, Phys. Rev. Lett., 1997, 79: 43
102. X. Y. Li, Q. Pan, J. T. Jing, J. Zhang, C. D. Xie, and K. C. Peng, Phys. Rev. Lett., 2002, 88: 047904
103. C. Schori, B. Julsgaard, J. L. Sorensen, and E. S. Polzik, Phys. Rev. Lett., 2002, 89: 057903
104. K. Honda, D. Akamatsu, M. Arikawa, Y. Yokoi, K. Akiba, S. Nagatsuka, T. Tanimura, A. Furusawa, and M. Kozuma, arXiv: 0709. 1785
105. H. Yonezawa, T. Aoki, and A. Furusawa, Nature, 2004, 431: 430
106. A. Furusawa and N. Takei, Phys. Rep., 2007, 443: 97
107. H. Wang, Q. Pan, Y. Zhang, C. Y. Xue, C. D. Xie, and K. C. Peng, Sci. China G, 1998, 41: 534
108. H. Wang, Y. Zhang, Q. Pan, H. Su, A. Porzio, C. D. Xie, and K. C. Peng, Phys. Rev. Lett., 1999, 82: 1414
109. P. H. Souto Ribeiro, C. Schwob, A. Maitre, and C. Fabre, Opt. Lett., 1997, 22: 1893
110. A. C. Funk and M. G. Raymer, Phys. Rev. A., 2002, 65: 042307
111. A. I. Lvovsky, H. Hansen, T. Aichele, O. Benson, J. Mlynek, and S. Schiller, Phys Rev. Lett., 2001, 87: 050402
112. J. Wenger, R. Tualle-Brouri, and P. Grangier, Phys. Rev. Lett., 2004, 92: 153601
113. A. Zavatta, S. Viciani, and M. Bellini, Science, 2003, 306: 660
114. A. Ourjoumtsev, R. Tualle-Brouri, and P. Grangier, Phys. Rev. Lett., 2006, 96: 213601
115. A. Ourjoumtsev, A. Dantan, R. Tualle-Brouri, and P. Grangier, Phys. Rev. Lett., 2007, 98: 030502
116. A. Ourjoumtsev, R. Tualle-Brouri, J. Laurat, and P. Grangier, Science, 2006, 312: 83
117. A. Ourjoumtsev, H. Jeong, R. Tualle-Brouri1, and P. Grangier, Nature, 2007, 448: 784
118. K. Wakui, H. Takahashi, A. Furusawa, and M. Sasaki, Opt. Express, 2007, 15: 13568